AD-A024 657

EFFECT OF THE CONSTRICTIVE AREA RATIO ON THE ROCKET EXHAUST FLOW-FIELD IN THE LAUNCHER

TEXAS UNIVERSITY AT AUSTIN

PREPARED FOR
ARMY MISSILE COMMAND

FEBRUARY 1976

THE UNIVERSITY OF TEXAS AT AUSTIN

EFFECT OF THE CONSTRICTIVE AREA RATIO ON THE ROCKET EXHAUST FLOW-FIELD IN THE LAUNCHER

John J. Bertin, Gena M. Garms, and Ed S. Idar, III

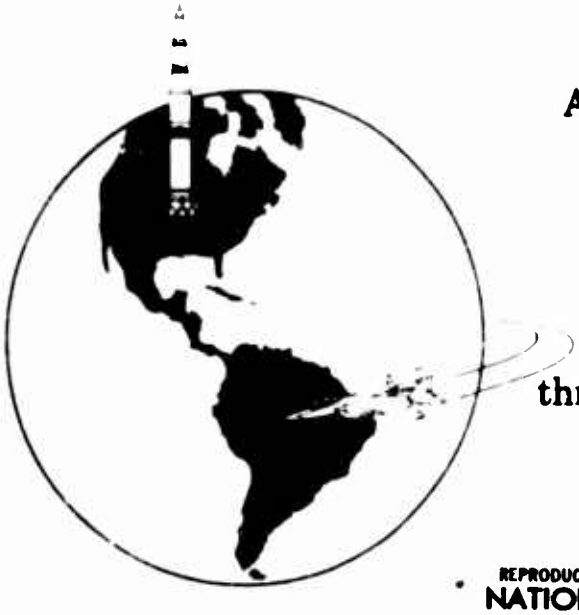

Aerospace Engineering Report 76001

This work was supported by the U.S. Army Missile Command through contract DAAH01-73-C-1016

February 1976

Department of Aerospace Engineering and Engineering Mechanics

EFFECT OF THE CONSTRICTIVE AREA RATIO ON THE ROCKET EXHAUST FLOW-FIELD IN THE LAUNCHER*

by John J. Bertin, Gena M. Garms, and
Ed S. Idar, III

Aerospace Engineering Report 76001

*This work was supported
by the U.S. Army Missile Command
through Contract DAAH01-73-C-1016

Department of Aerospace Engineering and
Engineering Mechanics

The University of Texas at Austin
February 1976

ACKNOWLEDGEMENTS

This analysis of flow field data for constrictive launch tubes was supported by the U.S. Army Missile Command (Huntsville, Alabama) through Contract DAAH01-73-C-1016. The authors acknowledge the considerable efforts of Mr. David Booker and Dr. James L. Batson in providing information about the relevant MICOM programs for which the University's tests would provide meaningful support and for technical direction to the University effort.

The authors would also like to thank Miss Bernadette Ashman and Mrs. Pat Kleinert for cheerfully typing the numerous drafts of the manuscript.

TABLE OF CONTENTS

INTRODUCTION

There are a variety of military rockets which are launched from variable-area launch tubes. The change in cross section allows the rocket to be initially constrained after ignition, while momentum is gained. The flow of the high temperature and high pressure rocket exhaust gas is of practical interest in the structural design of the launcher. Of special concern is the possible generation of unbalanced forces on the rocket by exhaust gases which are deflected upstream (i.e., blow-by flow) and which could influence the trajectory, once the rocket is released from its constraints. Flow in the so-called "non-tipoff" launch tubes is particularly complex since these tubes have diameter changes so that the rocket flies free of any tube support for a short distance as it emerges from the tube.

When the rocket exhausts directly into the small-diameter, aft tube, the flow downstream of the nozzle exit is entirely supersonic and intersecting, weak shock-waves occur. The resultant flow field is that for an underexpanded, supersonic jet exhausting into a constant-area tube having an inside diameter which is slightly larger than the nozzle exit. Fabri and Siestrunck (Ref. 1) found that the flow field in the tube varied with increasing rocket chamber pressure from mixed flow (subsonic and supersonic flow exist in the tube) with flow separation in the tube to fully developed supersonic flow throughout the tube (except, of course, in the viscous layers). Batson (Ref. 2) found that the static wall-pressure distributions in a constant-area tube which were obtained during a cold-gas test program were qualitatively similar to those obtained when a stationary rocket was exhausted into a constant-area tube. Batson and Bertin (Ref. 3) examined the tube-wall static-pressure distributions which were obtained when a rocket accelerated through an instrumented tube. The static-wall-pressures from these dynamic

rocket firings were qualitatively similar to the corresponding data from the static rocket firings of Ref. 2.

Significant blow-by flow was observed during an eight-flight test program in which Rip-Zap configurations were launched from a sparsely instrumented, non-tipoff launch tube. The constrictive launch tube, the launcher instrumentation, and the resultant data are described in Ref. 4. However, because of the paucity of test data, it was not possible to construct a flow model from these data. After these firings, personnel from the University of Texas at Austin entered the program. A more extensive instrumentation package for the launcher was designed for use in a subsequent series of four flights. Participation in the flight-test program by the University started with the specification of instrumentation for these four flights. The instrumentation package included static pressures, pitot pressures, and differential measurements of diametrically opposed static wall-pressures. A primary objective of this flight-test program was to obtain information which could be used to define important parameters for the flow field in the launcher. Of special interest was the identification of the source of blow-by flow. Two launcher geometries were included in the program. For one, the constrictive change in geometry was accomplished abruptly (i.e., a modified rectangular step); for the other, the area change was more gradual (i.e., a 15° ramp). For both configurations the cross-sectional area of the small-diameter, aft tube was 0.595 that of the forward tube. The flight-test data for this program have been discussed in Refs. 5 and 6.

Because of the complexity of the flow in the launcher, additional data were needed to construct a realistic flow model. To aid in the analysis of the data from the Rip-Zap launch program, two additional test programs have been conducted in which an underexpanded jet of unheated gas was exhausted from a stationary nozzle into a constrictive launch tube. The programs were

conducted at the U.S. Army Missile Command and at the University of Texas at Austin. The objectives of the cold-gas tests conducted at the U.S. Army Missile Command included the determination of the effect of reservoir pressure, nozzle-exit-position, and constrictive geometry on the blow-by mass-flow rate and on the static wall-pressure distribution in the launcher. The data from these tests were discussed in Ref. 7. When the nozzle exhausted directly into the small-diameter, aft tube, there was no significant blow-by flow. When the nozzle exhausted into the large-diameter, forward tube, significant blow-by flow was generated. For many test conditions, the blow-by flow in the annular region between the rocket and the launcher wall was transonic.

The cold-gas test program conducted at the University of Texas was designed to answer specific questions which arose during the analysis of the data from the Rip-Zap flight-test program (Refs. 5 and 6). The objectives of the cold-gas test program included the determination of the effect of vent ports located just upstream of the constriction and the determination of the parameters which govern the process by which flow downstream of the impingement shock is choked. Design considerations required immediate answers to the questions about the effect of vent holes. Therefore, for this phase of the test programs, the (quickly-built) launcher configuration simulated only a fraction of the length of the small-diameter, aft tube (i.e., the aft tube was, therefore, in reality a constrictive plug for the forward tube). However, the majority of the test program used a complete-length (but approximate) 0.2-scale model of the Rip-Zap launch tube. The geometry of the static nozzle which generated the required underexpanded, supersonic exhaust flow was the same for both phases of the test program. The data from this experimental program were presented in Ref. 8.

Experimental static-wall-pressure distributions were also obtained during launchings of the Arrow configuration, which were conducted at the U.S. Army

Missile Command Facility in Huntsville, Alabama. The cross-sectional area of the aft tube was 0.718 that of the forward tube for the Arrow launch tube. The pressure data indicated that there was not significant blow-by flow for the Arrow configuration (Ref. 9). Thus, a comparison of the data from the two flight-test programs demonstrates that the flow field in the launcher depends on the ratio of the nozzle-exit radius:aft-tube radius: forward-tube radius (as well as other parameters).

An experimental program has been conducted at the University of Texas in which unheated air was exhausted from an underexpanded nozzle into three different constrictive launch tubes. The primary variable of the test program was the diameter of the aft tube. Thus, for the present test-program, the cross-sectional area of the aft tube was 0.668, 0.735, and 0.878 of the area of the forward tube. The data for these three launcher configurations are discussed in the present paper.

NOMENCLATURE

A	cross-sectional area
M	Mach number
$\dot{m}$	mass-flow rate
p	static pressure
p_t	total pressure
r	radius
R	gas constant
T	static temperature
T_t	total temperature
u	streamwise velocity
x	axial coordinate
γ	ratio of specific heats
ρ	density
θ_{ne}	half-angle of the conical nozzle

Subscripts

aft	for the small-diameter, aft tube
ate	at the exit plane of the aft tube
ati	at the entrance plane (or initial station) of the aft tube
atm	atmospheric conditions
bb	for the blow-by flow
cyl	for the cylinder representing the external surface of the rocket
ds	downstream of the strong impingement shock
ex	for the flow exhausting through the nozzle
for	for the large-diameter, forward tube

ne	for the nozzle exit-plane
us	upstream of the strong impingement shock
1	for the reservoir chamber of the nozzle

EXPERIMENTAL PROGRAM

The objectives of the experimental program included the determination of the parameters which govern the generation of a strong shock wave which may occur when the exhaust flow impinges on the wall. Of special interest was the determination of the ratio of the radius of the aft tube (r_{aft}) to the radius of forward tube (r_{for}) for which the flow was no longer choked by the constriction. The variables of the test program included the total pressure in the nozzle stagnation chamber, the nozzle-exit-plane position, and the ratio $r_{aft}:r_{for}$ (or, equivalently, the constrictive area ratio $A_{aft}:A_{for}$).

The Facility

As shown in the sketch of Fig. 1, the cold-gas Rocket-Exhaust Effects Facility at the University of Texas at Austin consists of a high pressure supply system, a convergent-divergent nozzle (to simulate the rocket motor), and an instrumented, variable-area, launch tube. The instrumented tube could be moved axially to vary the location of the nozzle-exit-plane relative to the constriction and, thereby, to simulate (in a quasi-steady manner) the flow-fields which result when the rocket accelerates through the launcher. The assumption that the exhaust flow for the dynamic rocket launching is quasi-steady is based on the fact that the velocity of the exhaust gas is more than twenty times the velocity of the rocket as it leaves the launcher.

Photographs of the facility are presented in Fig. 2. The high pressure supply line (or feed pipe) which supplies air to the nozzle appears near the left center of the photograph of Fig. 2a. The launch tube is mounted on a movable table so that its location relative to the exit plane of the stationary nozzle is a parameter of the test program. For the present program the

nozzle axis and the launcher axis were colinear (although tipoff configurations can be simulated with the current apparatus). Also shown are the launcher instrumentation and the data monitoring systems. A close-up photograph of the "simulated" rocket positioned relative to the launch tube is presented in Fig. 2b. Note the pitot probe located in the annular region between the "simulated" rocket and the launcher wall. The probe is located at the upstream end of the forward tube in order to provide a measure of the mass-flow rate of the reverse, or blow-by, flow.

Nozzle. - A sketch of the convergent-divergent nozzle used in the present program is presented in Fig. 3. For this nozzle, the fairing between the convergent section and the conical divergent section was such that the throat radius of curvature was relatively small. If the flow is assumed to accelerate isentropically, the Mach number in the exit plane is 2.34 for the area ratio of the nozzle. However, shock waves which intersect at the nozzle axis in the vicinity of the nozzle-exit plane and which are evident in the schlieren photograph of the exhaust flow indicate that the acceleration of the flow in the conical divergent section was not an isentropic process. As suggested by Cline (Ref. 10), a possible source of the oblique shock wave is the discontinuity of the second derivative of the nozzle contour. A discussion of this shock is given in Ref. 11. It is possible to minimize (or to eliminate) this shock wave by increasing the radius of curvature or by contouring the throat curvature just upstream of the tangency point. Because of the presence of the shock waves, a series of tests were conducted in which pitot-pressure rakes were used to probe the flow from the nozzle-exit plane to four diameters downstream of the nozzle as it exhausted into a straight tube. For the present conical nozzle (i.e., $\theta_{ne} = 10°$), the transverse distributions of the experimentally-determined total-pressure were in approximate agreement with

the theoretical solutions obtained using a numerical code which assumed that the flow in the nozzle and that upstream of the weak, impingement shock wave was isentropic. For larger half-angle nozzles (i.e., $\theta_{ne} = 20°$), there were significant differences between the data (from the unreported tests) and the theoretical solutions. Therefore, no effort was made to alter the nozzle exhaust characteristics for the present test program.

Launch tubes. - The relevant dimensions of the three launch tubes are presented in Fig. 4 together with a sketch of the launcher and its instrumentation. The diameter of the aft tube was less than that of the forward tube. Hence, with the exit plane of the nozzle in the forward tube, the change in cross section served to constrict the flow of the exhaust gases. The change in geometry was accomplished by a rectangular step. The face of the step served as the origin of x (or axial) coordinate system. The coordinate system was such that x was positive for the aft tube and negative for the forward tube.

As has been discussed, these tests were conducted to determine the ratio of $A_{aft}:A_{for}$ for which the flow was no longer choked by the constriction. For the three launcher configurations of the present program, the cross-sectional area of the aft tube was 0.668, 0.735, and 0.878 of the area of the forward tube. The data from these configurations were intended to complement the data from the 0.2-scale Rip-Zap launcher, whose area ratio was 0.595 (refer to Ref. 8). Therefore, a single numbering system was used to identify the four tubes used in the two programs. Tube no. 1 identifies the Rip-Zap configuration (Ref. 8). Tubes 2 through 4 represent the three configurations of the present report. The constrictive area ratio, $A_{aft}:A_{for}$, increases with the tube number. The diameter of the forward tube was the same for all four tubes, i.e., 1.75 inches (4.45 cm). Thus, the variation in the area ratio was accomplished by varying the diameter of the aft tube. The specific values are presented in the table of Fig. 4.

Experience with the analysis of the flight test data for the Arrow launcher configuration, which had only six static-wall-pressure orifices (see Ref. 9), indicated that six gages would suffice if considerable a priori insight into the flow field was available. Thus, it was decided that the data from six static-wall-pressure orifices would be sufficient to "verify" the character of the flow field in the launcher. The use of the term "verify" presupposes that the flow field models which were developed in the analyses of Refs. 5, 8, and 9 will exist for the present configuration and can be identified with the pressure measurements from the six orifices. Three orifices were located in the small-diameter, aft tube and three in the large-diameter, forward tube. In each tube, one gage was located near the internal end, another near the middle, and the third near the external end. The overall length was 33.000 in. (83.820 cm.) for all three launcher configurations. The forward tube was nominally 15.0 in. (38.1 cm.) and the aft tube was nominally 18.0 in. (45.7 cm.). See Fig. 4 for details.

Data

The first step of the test procedure was to firmly position the launch tube so that the zero reference station was at the desired distance from the nozzle-exit plane. Furthermore, the axes of the nozzle and the launcher were colinear. The stagnation pressure in the nozzle reservoir and, therefore, the mass-flow-rate of the unheated air was controlled using the control valve of Fig. 1. The minimum value of stagnation pressure in the nozzle reservoir (p_{t1}) for which data were recorded was approximately 200 psia (1.38×10^6 N/m^2). At this value of p_{t1}, the theoretical value (for isentropic flow) of the static pressure in the nozzle-exit plane was approximately equal to the atmospheric pressure. Through periodic adjustments of the control valve, the stagnation pressure was increased to another value, held constant while the data were

recorded, and increased again up to a maximum of 1000 psia (6.90×10^6 N/m^2). Approximately 5 seconds were required to obtain the required data at a particular stagnation pressure. The experimental data obtained during a run included the static-wall-pressure distribution, the stagnation pressure in the nozzle reservoir, the total pressure of the reverse (or blow-by) flow in the annular region, and (for certain tests) schlieren photographs.

Static-wall-pressure. - The locations and dimensions of the static-wall-pressure orifices were discussed in the previous section. The static-wall-pressures were measured using either bourdon-type dial gages or potentiometer-type transducers. The bourdon-type gages used had ranges of 0 to 30 psig, 0 to 60 psig, -14.7 to 100 psig, -14.7 to 50 psig, 0 to 200 psig, 0 to 45 psig, and 0 to 2000 psig. The pressure ranges for the transducers were 0 to 45 psig, 0 to 100 psia, 0 to 600 psia, 0 to 1000 psia, and 0 to 3000 psia. The output from the dial-type gages were recorded photographically. The output from the transducers was recorded using either strip chart recorders or on an oscillograph (See Fig. 2a). Because the number of orifices exceeded the number of gages available, it was necessary to run more than once to obtain a complete distribution for a particular nozzle position.

Blow-by mass-flow-rate. - An estimate of the blow-by mass-flow-rate was made using the pressure data from the pitot probe located in the annular region between the "rocket" nozzle and the launch tube (see Fig. 2b). In order to obtain numerical values, the variations of the local flow properties across the annular region were neglected for the present calculations. Thus,

$$\dot{m}_{bb} = \rho_{bb} u_{bb} \pi (r_{for}^2 - r_{cyl}^2) \tag{1}$$

For a perfect gas

$$\rho_{bb} = \frac{p_{bb}}{RT_{bb}} \tag{2}$$

and

$$u_{bb} = M_{bb}\sqrt{\gamma RT_{bb}} \tag{3}$$

Since the blow-by flow was found to be subsonic, the static pressure at the forward exit-plane of the launcher was atmospheric (which was verified by the static-wall-pressure measurements from this region). The ratio p_{bb}/p_{tbb} was used to calculate the blow-by Mach number (Ref. 12). If one assumes that the flow was adiabatic from the reservoir, through the nozzle, and through the flow reversal, the energy equation yields

$$\frac{T_t}{T_{bb}} = 1 + \frac{\gamma - 1}{2} M_{bb}^2 \tag{4}$$

Of primary interest is the fraction of the nozzle exhaust flow which was reversed. The mass flow of the "rocket" nozzle exhaust is given by:

$$\dot{m}_{ex} = \frac{p_{t1}}{\sqrt{T_t}}\sqrt{\frac{2\gamma}{R(\gamma+1)}}\left(\frac{2}{\gamma+1}\right)^{\frac{1}{\gamma-1}} \pi(r^*)^2 \tag{5}$$

Thus, the dimensionless blow-by mass-flow-rate is:

$$\frac{\dot{m}_{bb}}{\dot{m}_{ex}} = M_{bb}\sqrt{\frac{T_t}{T_{bb}}}\,\frac{p_{bb}}{p_{t1}}\,\frac{(r_t^2 - r_{cyl}^2)}{\sqrt{\frac{2}{\gamma+1}}\left(\frac{2}{\gamma+1}\right)^{\frac{1}{\gamma-1}}(r^*)^2} \tag{6}$$

For the geometry of the current test program, which used unheated air as the test gas:

$$\frac{\dot{m}_{bb}}{\dot{m}_{ex}} = 4.41384\; M_{bb}\sqrt{\frac{T_t}{T_{bb}}}\,\frac{p_{bb}}{p_{t1}} \tag{7}$$

Schlieren photographs. - The facility has an all-lens schlieren system which was used during certain runs to study the flow as it exhausted from the an-

nular region at the forward exit-plane of the launcher or from the vent ports. Schlieren photographs were also taken of the nozzle exhaust flow (refer to Fig. 3).

Test Program

As noted earlier, the variables of the test program included the total pressure in the nozzle stagnation chamber, the nozzle-exit-plane position, and the ratio $r_{aft}:r_{for}$. Data were obtained over the range of reservoir stagnation pressure from 200 psia (1.38×10^6 N/m^2) to 1000 psia (6.90×10^6 N/m^2). As can be seen in the run schedule presented in Table 1, the nozzle exhausted directly into the small-diameter, aft tube for some tests, i.e., $x_{ne} = +1.00\ r_{ne}$. However, for the majority of the runs, the nozzle exhausted into the large-diameter forward tube. The nozzle-exit positions investigated were such that $-19.25\ r_{ne} \leq x_{ne} \leq +1.00\ r_{ne}$. It should be noted that two or three runs were conducted for each rocket-nozzle location/launcher configuration indicated in Table 1. In each case, the measurements from the repeat runs were in essential agreement with each other. For launcher 2, A_{aft} was $0.668\ A_{for}$; for the launcher 3, A_{aft} was $0.735\ A_{for}$; and for launcher 4, A_{aft} was $0.878\ A_{for}$.

DISCUSSION OF RESULTS

The static-wall-pressure distributions obtained during the Rip-Zap flight test program (for which $A_{aft} = 0.595\ A_{for}$) indicate that the exhaust flow was choked by the constriction, a strong shock wave was generated when the flow impinged on the wall and the downstream flow was subsonic. The large adverse pressure gradient produced by the strong shock wave caused a significant fraction of the flow in the impinging shear layer to be turned upstream (which is termed the reverse, or blow-by, flow). The static-wall-pressure distributions obtained during the Arrow flight-test program (for which $A_{aft} = 0.718\ A_{for}$) indicate that the exhaust flow remained supersonic. As a result, there was not significant blow-by flow. Using cold-gas data obtained in the University's Rocket-Exhaust Effects Facility, a flow model was developed which described the choked flow in the launcher. Despite the simplicity of the flow model, the theoretical pressures were in excellent agreement with the cold-gas data for the 0.2-scale model tests and were in fair agreement with the flight-test data. A sketch of the proposed flow model is presented in Fig. 5. The relative dimensions of nozzle-exit radius (r_{ne}): aft-tube radius (r_{aft}):forward-tube radius (r_{for}) are to scale. The axial dimensions are not to scale. Thus, whereas the impingement shock wave is sketched as a normal shock wave extending almost from wall to wall, oblique shock waves associated with the initial turning of the flow probably extended over a longer distance than indicated in the sketch. The extent over which the pressure rise occurred would be a measure of the interaction between the viscous shear layer and the complex shock-wave structure. The essential features of the flow model include: (1) the underexpanded flow in the nozzle exit plane (designated by the subscript ne), (2) the supersonic flow just upstream of the impingement shock wave (designated by the subscript us), (3) the subsonic flow just

downstream of the strong impingement shock wave (designated by the subscript ds), (4) the reverse, or blow-by, flow (i.e., that fluid in the viscous shear layer which cannot overcome the adverse pressure gradient generated by the interaction between the impingement shock and the viscous flow), (5) the region at the base of the step where some of the fluid which has passed through the shock system stagnates, (6) the subsonic flow at the entrance of the small-diameter, aft tube (designated by the subscript ati), and (7) the sonic flow at the exit plane of the small-diameter, aft tube (designated by the subscript ate).

Since the data for launcher configuration 2 (for which $A_{aft} = 0.668\ A_{for}$) indicate that the flow field was qualitatively similar to that (described above) for the Rip-Zap configuration (i.e., launcher configuration 1), they will be presented first. After discussing the data for launcher configurations 3 and 4, correlations indicating the effect of the constrictive area ratio will be presented.

Launcher Configuration 2

As was the case for launcher configuration 1 (i.e., the 0.2-scale Rip-Zap launcher), the blow-by flow rates for launcher configuration 2 can be used to define the range of nozzle exit positions for each of three characteristics regions. The blow-by mass-flow-rate divided by the total flow through the nozzle is presented as a function of the nozzle-exit position in Fig. 6 for $p_{t1} \approx 950$ psia (6.55×10^6 N/m^2). Based on these data, the three characteristic regions are as follows.

(1) Region 1: For $x_{ne} > 0$, the downstream flow remained entirely supersonic and the blow-by mass-flow-rate was negligible. Only that portion of the fluid in the shear layer which could not overcome the relatively small adverse pressure gradient associated with the weak, impingement shock wave was turned upstream.

(2) Region 2: For $-6\ r_{ne} < x_{ne} < 0$, the mass-flow-rate varied rapidly with nozzle location. When $x_{ne} = -1.0\ r_{ne}$, $\dot{m}_{bb}$ was approximately $0.07\ \dot{m}_{ex}$. For $-4.16\ r_{ne} \leq x_{ne} \leq -2.35\ r_{ne}$, $\dot{m}_{bb}$ was approximately $0.05\ \dot{m}_{ex}$. This position-dependent variation is believed to be similar to the puff of blow-by flow observed during the Rip-Zap flight-test program (Ref. 6). For $-6.41\ r_{ne} \leq x_{ne} < -4.16\ r_{ne}$, the blow-by mass-flow-rate increased with distance from the face of the rectangular step.

(3) Region 3: When the exit plane was well into the forward tube, i.e., $x_{ne} < -6.5\ r_{ne}$, the flow downstream of the impingement shock wave was choked by the constrictive change in cross section. The normal shock wave which was generated when the exhaust flow impinged on the wall caused a rapid increase in pressure in the streamwise direction. This large, adverse pressure gradient caused a considerable portion of the fluid in the viscous layer to be turned upstream into the annular region. With the exception of the measurements obtained when x_{ne} was $-15\ r_{ne}$, the blow-by flow rate was essentially independent of nozzle position at this value of the stagnation pressure, i.e., approximately 950 psia (6.55×10^6 N/m^2). Whether the relatively low blow-by flow rates obtained for $x_{ne} = -15.0\ r_{ne}$ were due to experimental error or to some unexplained flow mechanism is not known. However, the relatively large scatter in the data and the fact that a similar phenomena was not observed for launcher configuration 1 indicate experimental error.

Also presented in Fig. 6 are data from experimental programs where an unheated gas was exhausted into a constrictive launcher with $A_{aft} = 0.595\ A_{for}$ (i.e., the Rip-Zap configuration, or launcher configuration 1). For $-5\ r_{ne} < x_{ne} < 0$, $\dot{m}_{bb}$ increased with distance from the step for the 0.2-scale launcher of Ref. 8 (based on the <u>two</u> locations tested) but decreased from the MICOM configuration with the rectangular-step (i.e., the launcher of Ref. 7). Note, however, that the 0.38 scale launcher of Ref. 7 simulated only $4.19\ r_{ne}$ of the

forward tube, whereas the launcher of Ref. 8 simulated the entire length. As a result, the forward tube was much shorter and the dimension of the annular gap larger for the launcher of Ref. 7. Thus, in Ref. 8 the principal author observed that "the viscous effects were significantly different for the two rectangular-step configurations. Whether the differences in the viscous effects explains the apparent anomaly in the blow-by data of Fig. 6 is not known". For $-4\ r_{ne} \leq x_{ne} < 0$, the blow-by flow rates decreased with distance from the step for launcher configuration 2, which supported the data of Ref. 7. Furthermore, the blow-by flow rates were equal for the two Rip-Zap launchers (i.e., those of Refs. 7 and 8) when x_{ne} was approximately $-2.4\ r_{ne}$ (which was the only nozzle-exit location tested for launcher configuration 1 in the range $-4\ r_{ne} \leq x_{ne} < 0$). Thus, the apparent discrepancy between the blow-by data for the two launchers with $A_{aft} = 0.595\ A_{for}$ was not a discrepancy at all. Instead, with the additional insight provided by the data of the present tests, it is believed that had more data been available for the configuration of Ref. 8, the correlation between blow-by flow rate and nozzle-exit location would have been the same for both Rip-Zap launchers.

The pressure distributions measured for configuration 2 with $x_{ne} = -2.35\ r_{ne}$ are compared with the data for configuration 1 (i.e., the Rip-Zap configuration of Ref. 8) in Fig. 7a. For $p_{tl} < 437$ psia (3.02×10^6 N/m^2), the data were qualitatively similar for the two configurations. At these relatively low stagnation pressures, the theoretical value of the static pressure in the nozzle exit-plane (assuming isentropic flow in the nozzle) was "approximately" equal to the atmospheric value. The exhaust flow apparently impinged on the face of the step, producing the pressure increase evident at the base of the step. The resultant pressure gradient from the internal end of the forward tube (i.e., $x = 0$) to the forward end of the launcher (i.e., $x = -26.6\ r_{ne}$) apparently was not sufficient to produce a significant blow-by flow-rate.

For $p_{t1} \geq 506$ psia (3.49×10^6 N/m^2), the pressure in the exit-plane of the nozzle was so much greater than the atmospheric value that the exhaust flow impinged on the wall as it expanded into the forward tube. Downstream of the impingement shock, the pressure increased, reaching a maximum at the base of the step. Thus, the impinging exhaust flow encountered a large adverse pressure gradient which caused a significant portion of the fluid to be turned upstream, i.e., to be reversed. The mass-flow rate of the reverse, or blow-by, flow was approximately 5 per cent of the mass-flow-rate through the nozzle (see Fig. 6). The blow-by flow rate was sufficient to produce nonatmospheric values for the static-wall-pressure measurements in the annular region between the rocket and the wall of the forward tube. However, since the reverse flow was subsonic, the static pressure at the forward end of the annular region was equal to the atmospheric value. The experimental static pressures from the aft tube are significantly less than the values obtained in tests where the flow in the aft-tube was subsonic, e.g., Fig. 7d. Thus, it is believed that the flow in the aft tube was supersonic over the entire range of p_{t1} for $x_{ne} = -2.35\ r_{ne}$.

The pressure measurements for $x_{ne} = -6.41\ r_{ne}$, $-10.41\ r_{ne}$, $-15.00\ r_{ne}$ and $-19.25\ r_{ne}$ are presented in Figs. 7b through 7e. For a given nozzle-exit location, the pressure distribution changed character when the stagnation pressure (or, equivalently, the mass-flow rate through the nozzle) was above a critical value. The critical value was a function of nozzle-exit-position. As a result of the changes in the mass flow-rate, in the strength of the impingement shock, and in the fluid properties downstream of the impingement shock wave, the flow was choked by the constriction. A strong shock wave was generated in the region where the exhaust flow impinged on the wall. The fact that the static pressure decreased as the flow passed through the constriction indicated that the flow downstream of the impingement shock-wave was subsonic. Recall that, if $dA < 0$, subsonic flow accelerates while supersonic flow decelerates.

The interaction between the strong shock wave and the viscous shear layer created a large pressure gradient which caused a large fraction of the flow to be turned upstream. Thus, the exhaust flows which produced the pressure data presented in Figs. 7b-7e correspond to the flow model presented in Fig. 5.

To substantiate the validity of the flow model for the choked flow of Region 3, let us compare the experimental pressures of Figs. 7c-7e with the corresponding theoretical values. The theoretical values assume a one-dimensional flow incorporating the phenomena of Fig. 5. The one-dimensional exhaust flow was assumed to accelerate isentropically from the sonic conditions at the throat to the conditions just upstream of the shock. Since A_{for} was $5.302A^*$, M_{us} was 3.237 (see Ref. 12). Downstream of the normal shock-wave the theoretical Mach number (M_{ds}) was 0.4626 and the theoretical static pressure (p_{ds}) was 0.2147 p_{t1}. The theoretical value for the static pressure was in reasonable agreement with the experimental values of Fig. 7e (the experimental values were approximately 0.22 p_{t1}). The theoretical stagnation-pressure downstream of a normal shock-wave (0.2676 p_{t1}) was in reasonable agreement with the pressures measured at the base of the rectangular step. Thus, (1) there was reasonable agreement between the experimental data and the theoretical values (for the relatively crude approximations), (2) the location of the normal shock wave was fixed with respect to the nozzle exit-plane, and (3) the choked flow-by flow rate was independent of nozzle-exit location. These three observations support the conclusion (as illustrated in Fig. 5) that the fluid which constituted the blow-by flow did not pass through the shock system.

The drop in pressure indicated that the flow accelerated through the constriction (and was, therefore, subsonic). The model for the resultant flow in the aft tube appears to be that described by Shapiro (Ref. 13) as choking due to friction. That the flow in the exit plane of the aft tube was indeed sonic was indicated by the static pressure measurements (see Fig. 7e). Assuming that

the fluid near the center of the launcher accelerated isentropically from "ds", the static pressure at the sonic location would have been 0.5283 p_{t2}, or 0.1414 p_{t1}. This value for the theoretical static pressure at the sonic location was essentially equal to the static-pressure measurements from near the exit plane of the aft tube.

Launcher Configuration 3

The constrictive area ratio, A_{aft}/A_{for}, for launcher configuration 3 was 0.735. Thus, the constrictive area ratio was close to that for the Arrow launch tube (which was 0.718). However, whereas no significant blow-by flow was observed during the Arrow flight-test program, such was not the case when unheated air was exhausted into launcher configuration 3. Parameters which differed between the cold-gas simulation and the rocket launching included the following.

(1) Constrictive area ratio: 0.718 for the Arrow launch tube, 0.735 for launcher configuration 3

(2) Constrictive geometry: 4° ramp by the Arrow launch tube, rectangular step for launcher configuration 3

(3) γ: 1.18 for the Arrow rocket, 1.40 for the University's cold-gas facility

(4) Nozzle half-angle: 5° for the Arrow rocket, 10° for the rocket exhaust effects facility.

The nondimensionalized blow-by mass-flow-rates are presented in Fig. 8 as a function of the nozzle-exit location for the highest value of the stagnation pressure at which data were obtained, i.e., $p_{t1} \approx 950$ psia (6.55×10^6 N/m^2). As was the case for launcher configurations 1 and 2, a significant, position-dependent blow-by flow occurred as the nozzle exit-plane entered the forward tube. The nondimensionalized blow-by mass-flow-rates for launcher configuration 3 are significantly less than the values for launcher configura-

tions 1 and 2 (refer to Fig. 6). The variation in the magnitude of the blow-by flow as the nozzle moved from the step has been described as a puff. For $-10.41\ r_{ne} \leq x_{ne} \leq -6.41\ r_{ne}$, i.e., when the nozzle exit-plane was in the middle of the forward tube, the blow-by flow rate was negligible. The lack of measureable blow-by flow indicated that the impingement shock wave was weak and that the flow downstream of the impingement shock and into the aft tube remained supersonic. These conclusions based on the blow-by measurements were substantiated by the static-wall-pressure measurements, which are presented in Figs. 10b and 10c. Thus, for these two nozzle positions, the cold-gas data were consistent with the Arrow flight-test data.

When the nozzle exit-plane was positioned further from the step, the blow-by flow rate increased dramatically. For $x_{ne} \leq -15.00\ r_{ne}$, the blow-by flow rate was constant at a "relatively high" value. Thus, the exhaust flow had apparently choked as it encountered the constriction. Since the exhaust flow did not choke until the nozzle exit-plane was $15.00\ r_{ne}$, or more, into the forward tube, the reduction of the effective cross-section due to the growth of the viscous boundary-layer contributed to the choking of the flow.

The nondimensionalized blow-by mass-flow-rates are presented in Fig. 9 as a function of the reservoir stagnation pressure (for all six nozzle-exit locations). As noted previously, the Mach number in the exit plane would be 2.34 if the flow in the nozzle expanded isentropically. Therefore, the flow in the nozzle would be overexpanded for $p_{t1} \leq 200$ psia (1.38×10^6 N/m^2). Data are not presented for the overexpanded nozzle flows, since they were not relevant to the applications of the present study. For $x_{ne} = -1.00\ r_{ne}$, the nondimensionalized blow-by flow rate was constant for $p_{t1} > 400$ psia (2.76×10^6 N/m^2). The exhaust flow impinged directly on the face of the constrictive step producing a pressure gradient along the annular region between the rocket and the launcher wall. The pressure drop from the face of the step to the

atmospheric value at the forward (external) end of the forward tube was sufficient to turn approximately 5% of the exhaust flow upstream. For $x_{ne} = -2.35\ r_{ne}$, the nozzle exit-plane was far enough into the forward tube that the exhaust flow impinged on the wall upstream of the step. The majority of the exhaust gases passed through the "weak" impingement shock-wave system. The fraction of the exhaust flow which did not have sufficient momentum to overcome the adverse pressure gradient associated with the impingement shock wave was negligible for $p_{tl} \leq 700$ psia (4.83×10^6 N/m^2). The nondimensionalized blow-by flow rate increased with p_{ti} for $p_{tl} > 700$ psia (4.83×10^6 N/m^2). Although the mechanism which generated the pressure-dependent blow-by flow for this nozzle-exit location is not understood, the nondimensionalized static pressure recorded at the orifice located in the wall just upstream of the step was also significantly greater for $p_{tl} > 700$ psia (4.83×10^6 N/m^2). For $x_{ne} = -6.41\ r_{ne}$ or $-10.41\ r_{ne}$, the blow-by mass-flow-rate was insignificant over the entire range of reservoir pressures tested. As noted, the lack of significant blow-by flow was consistent with the data from the Arrow flight-test program. However, for $x_{ne} \leq -15\ r_{ne}$, a significant portion of the exhaust flow was turned upstream over the entire range of reservoir stagnation pressure tested. As evident in the static-wall-pressure distributions (refer to Figs. 10d and 10e), the impingement shock wave was strong. The downstream flow was subsonic as indicated by the acceleration of the flow through the constriction (i.e., the pressure decreased).

Based on previous flight-test data (Ref. 6) and cold-gas data (Ref. 8), the difference in the geometry of the constriction should not significantly alter the flow in the launcher. It is possible, however, that the constrictive geometry would affect the internal flow-field for launcher configurations where the total reduction in the effective cross-section due to the boundary layer and to the constriction first causes the flow to choke. Since the constrictive area ratio was greater for launcher configuration 3 than for the Arrow config-

uration, the fact that the flow choked was surprising. However, the differences in γ and the conical-nozzle half-angle would cause the impingement shock structure to be different. Rip-Zap flight-test data dramatically illustrated (Ref. 5) how the exhaust flow characteristics and the resultant changes in the impingement shock structure could produce radical changes in the internal flow field. Because the cold-gas flow choked only when the nozzle was far into the forward tube, it is believed that the growth of the viscous boundary-layer significantly affected the choking process.

The static-wall-pressure distributions obtained for launcher configuration 3 are presented in Fig. 10. It has been concluded that, for $x_{ne} \geq -10.41\ r_{ne}$, the exhaust flow remained supersonic as it passed the constriction and through the aft tube. This conclusion is supported by the fact that the static pressure increased as the flow passed through the constriction (since supersonic flow decelerated for $dA < 0$). Thus, a pattern of weak shock waves reflecting across the tube produced periodic increases in pressure along the tube. The shock-induced pressure variations are evident in the pressure measurements of Figs. 10a-10c. For $x_{ne} = -2.35\ r_{ne}$, the static wall-pressure measurements for the orifice just downstream of the nozzle exit location were in reasonable agreement with the theoretical pressure immediately downstream of the weak, impingement shock-wave, which was $0.075\ p_{t1}$. The theoretical value was calculated assuming that the underexpanded flow in the nozzle exit-plane expanded to the base pressure, which was atmospheric, and was turned parallel to the wall by a weak oblique shock wave. Viscous effects were neglected. Because of the location of the nozzle-exit plane relative to the orifice locations for the other nozzle positions, i.e., Figs. 10b and 10c, the local peak pressure just downstream of the impingement shock wave.

For $x_{ne} \leq -15.00\ r_{ne}$, the combined constrictive effect of the boundary layer and of the change in cross section caused the flow to choke. The static-wall-pressure distributions presented in Figs. 10d and 10e verify that the impinge-

ment shock wave was strong so that the downstream flow was subsonic. The experimentally-determined pressures are in reasonable agreement with the theoretical values for the one-dimensional flow model of Fig. 5.

Launcher Configuration 4

The constrictive area ratio for launcher configuration 4 was 0.878. The nondimensionalized blow-by mass-flow-rate measured when p_{t1} was approximately 950 psia (6.55×10^6 N/m^2) is presented in Fig. 11 for all nozzle-exit locations for which data were obtained. The blow-by flow rate was negligible for all exit locations. Based on the data for the other launch tubes, the negligible blow-by flow rates were expected.

The static-wall-pressure distributions, which are presented in Fig. 12, show that the pressure increased (albeit slightly) as the supersonic flow decelerated through the constriction. No pressure greater than 0.06 p_{t1} was measured. Note that the theoretical static pressure downstream of the weak impingement shock wave for the forward tube was 0.07 p_{t1}. Furthermore, static pressures for orifices in the aft tube which were measuring during the Arrow flight test program (Ref. 14) were measurably above the shock impingement value. Thus, the experimental values presented in Fig. 12 were lower than expected. Because there were only a limited number of orifices available it is possible that the orifices recorded only the relatively low values which exist between the reflecting shock waves. Since each test condition was repeated without significant changes in the pressure data, the measured values are believed to be valid. If the measured pressures are indeed low in comparison to the "theoretical" flow models used to date, the flow mechanism unique to launcher configuration 4 is not understood.

The Effect of Constrictive Area Ratio

Nondimensionalized blow-by mass-flow-rates are presented as a function of

the constrictive area ratio for x_{ne} = -2.35 r_{ne}, -10.41 r_{ne}, and -19.25 r_{ne} in Figs. 13, 14, and 15, respectively. Based on these data, the following conclusions are made.

(1) The stagnation pressure did not significantly affect the nondimensionalized blow-by mass-flow-rate for these two stagnation pressures. An exception to this conclusion is evident in Fig. 13a. When A_{aft}/A_{for} was 0.595 and x_{ne} = -2.35 r_{ne}, the blow-by flow rate was very sensitive to the reservoir stagnation pressure for values near 400 psia (2.76×10^6 N/m^2).

(2) The fraction of the exhaust flow which was turned upstream by the adverse pressure gradient created by the strong impingement shock wave generated when the flow choked increased as the diameter of the aft tube decreased.

(3) The constrictive area ratio required to choke the flow was a function of nozzle-exit location.

CONCLUDING REMARKS

Static wall-pressure distributions have been measured when an underexpanded jet of unheated air was exhausted into a constrictive launch tube. The corresponding blow-by rate was determined using a pitot probe located in the annular region between the simulated rocket and the launcher wall at the exit plane of the forward tube. Based on these data, the following conclusions are made:

(1) The stagnation pressure did not significantly affect the fraction of the exhaust flow turned upstream for reservoir pressures in excess of 400 psia (2.76×10^6 N/m^2).

(2) The fraction of the exhaust flow which was turned upstream by the adverse pressure gradient created by the strong impingement shock wave generated when the flow choked increased as the diameter of the aft tube decreased.

(3) The constrictive area ratio required to choke the flow was a function of the nozzle-exit location.

It might also be noted that the data from these cold-gas simulations were in essential agreement with the data from flight-test programs.

REFERENCES

1. Fabri, J., and Siestrunck, R.: "Supersonic Air Ejectors", Advances in Applied Mechanics, Vol. V, Academic Press, Inc., New York, 1958, pp. 1-34.

2. Batson, J.L.: "A Study of the Flow Field Produced by an Axisymmetric Underexpanded Jet Exhausting into a Cylindrical Tube", Ph.D. Dissertation, December 1972, The University of Texas at Austin.

3. Batson, J.L., and Bertin, J.J.: "Experimental Study of Flow Field Produced When an Underexpanded Rocket Exhausts into Cylinder Tube", AIAA Paper No. 73-1227, Presented at AIAA/SAE 9th Propulsion Conference, Las Vegas, November 1973.

4. ————————: "Feasibility Flight Testing of Rocket Impelled Projectile (RIP)", Report Number 7-52100/3R-5, 1 May 1973, LTV Aerospace Corporation, Michigan Division.

5. Bertin, J.J. and Reiman, R.A.: "The Analysis of the Launch-Tube Flow-Field for Rip-Zap Firings", Aerospace Engineering Report 74005, October 1974, The University of Texas at Austin.

6. Bertin, J.J., and Batson, J.L.: "Experimenatlly Determined Rocket-Exhaust Flowfield in a Constrictive Tube Launcher", Journal of Spacecraft and Rockets, December 1975, Vol. 12, No. 12.

7. Bertin, J.J., Horn, M.K., and Webber, T.L.: "Experimental Study of Flow Field Produced When an Underexpanded Jet Exhausts into a Constrictive Stepped Launch Tube", Aerospace Engineering Report 74002, January 1974, The University of Texas at Austin.

8. Bertin, J.J., Morris, R.R., Garms, G.M., Motal, M.R., and Faria, H.T.: "Experimental Study of an Underexpanded, Supersonic Nozzle Exhausting Into A Constrictive Launch Tube", Aerospace Engineering Report 75001, June 1975, The University of Texas at Austin.

9. Bertin, J.J., and Galanski, S.R.: "The Analysis of Launch Tube Flow-Field for Arrow Firings", Aerospace Engineering Report 75004, May 1975, The University of Texas at Austin.

10. Cline, M.C.: Private transmittal, July 3, 1974, University of California Los Alamos Scientific Laboratory, Los Alamos, New Mexico.

11. Back, L.H., and Cuffel, R.F.: "Detection of Oblique Shocks in a Conical Nozzle with a Circular-Arc Throat", AIAA Journal, December 1966, Vol. 4, No. 12, pp. 2219-2221.

12. Ames Research Staff: "Equations, Tables, and Charts for Compressible Flow", Report 1135, 1953, NACA.

13. Shapiro, A.H., The Dynamics and Thermodynamics of Compressible Fluid Flow, Ronald Press, 1953, New York.

14. Bertin, J.J., and Batson, J.L., "A Comparison of Cold-Gas Simulation and Rocket-Launch Data for Constrictive Launchers", to be published.

Table 1.-Test Configurations

Launcher*	$\frac{x_{ne}}{r_{ne}}$												
	+1.00	-1.00	-2.35	-3.00	-4.16	-5.00	-6.41	-7.50	-8.41	-10.41	-13.00	-15.00	-19.25
2	X	X	X	X	X	X	X	X	X	X	X	X	X
3		X	X				X			X		X	X
4	X	X	X		X		X		X	X		X	X

*Refer to Figure 4 for the geometry of the launcher configurations.

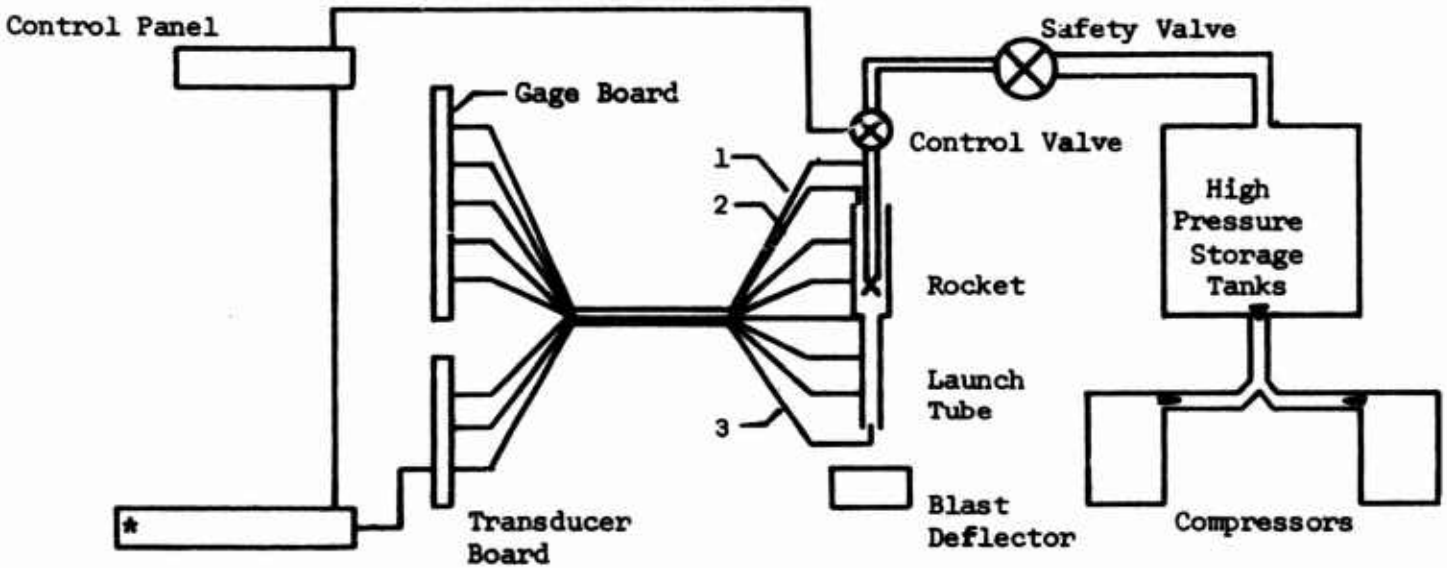

Figure 1.- Schematic of the University of Texas Rocket-Exhaust Effects Facility.

(a) Overall view of facility

Figure 2. - Photographs of the cold-gas Rocket-Exhaust Effects Facility at the University of Texas at Austin.

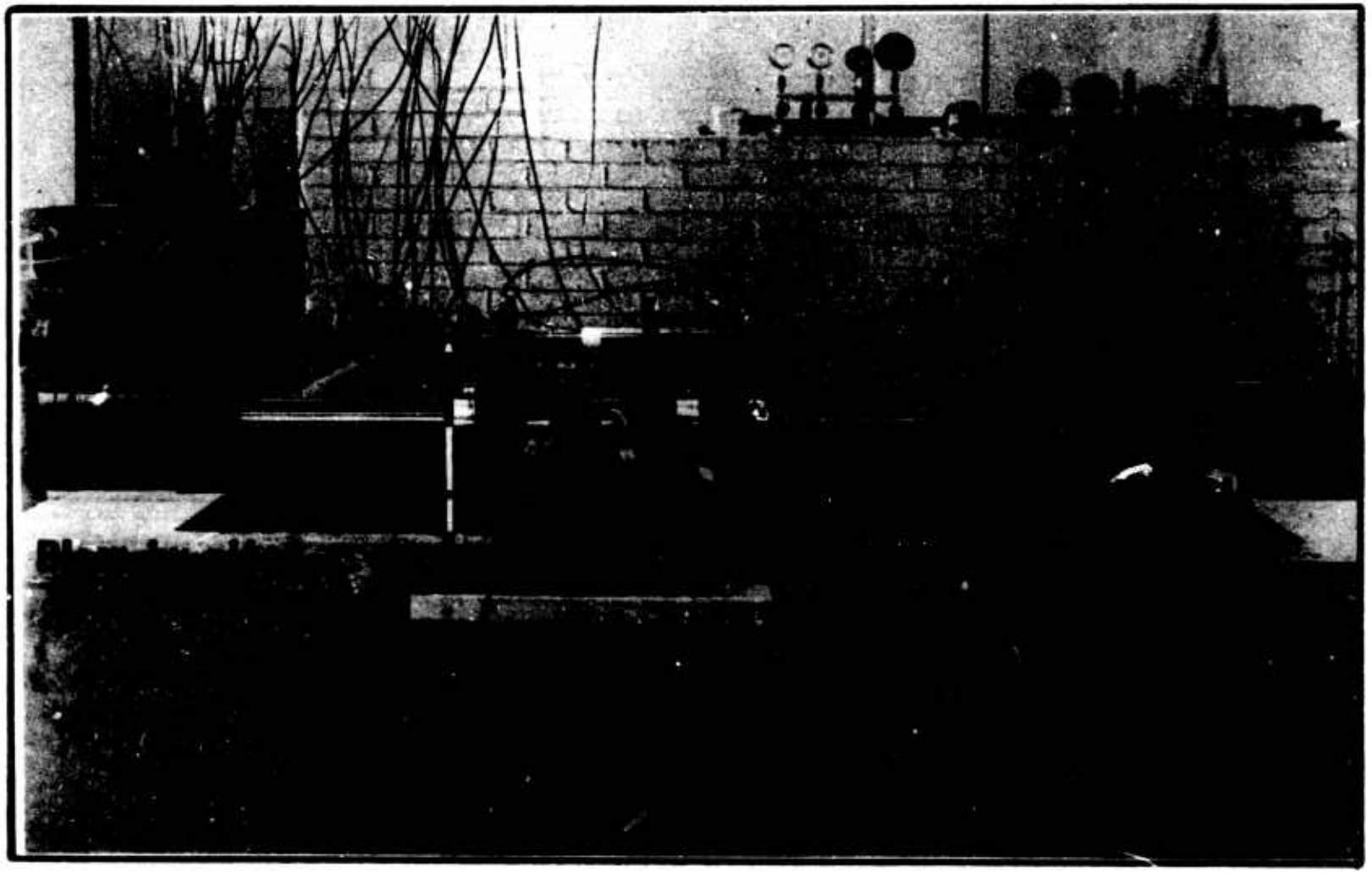

(b) Close-up of "rocket" and "launch tube"

Figure 2. - Concluded.

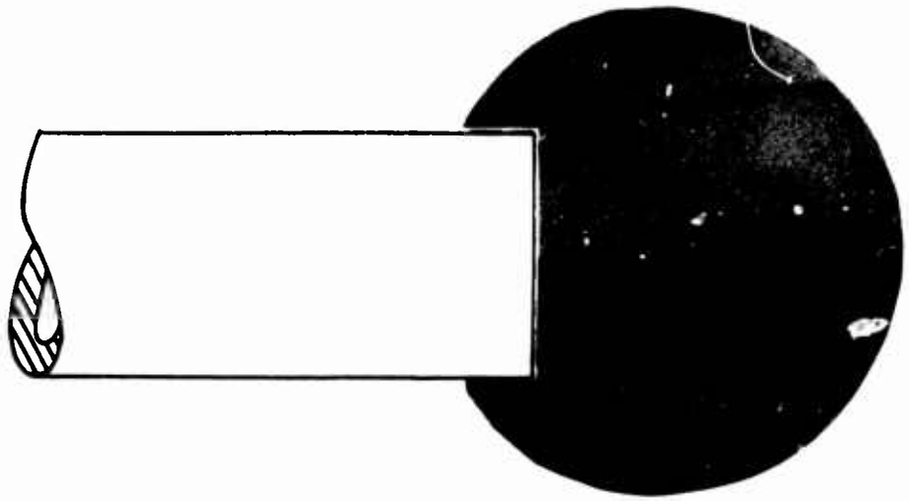

(a) Schlieren photograph of the nozzle exhaust flow.

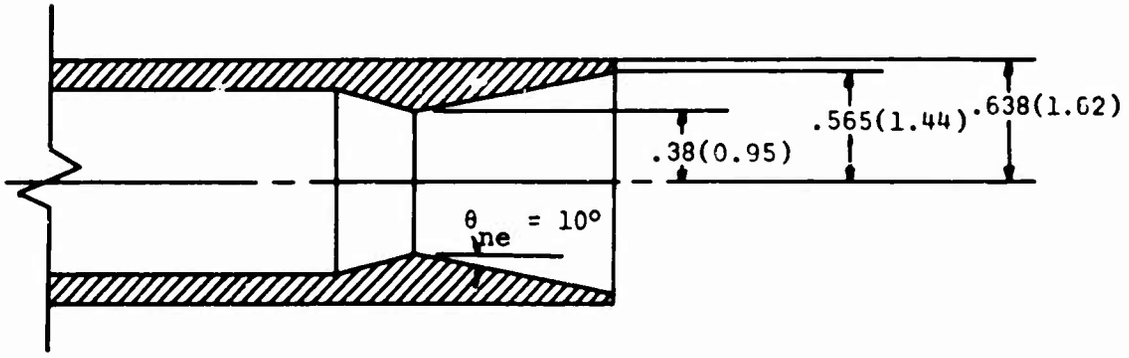

Note: dimensions in inches (centimeters)

(b) Dimensions of the convergent-divergent nozzle.

Figure 3. - Characteristics of the convergent-divergent nozzle used during the cold-gas test program.

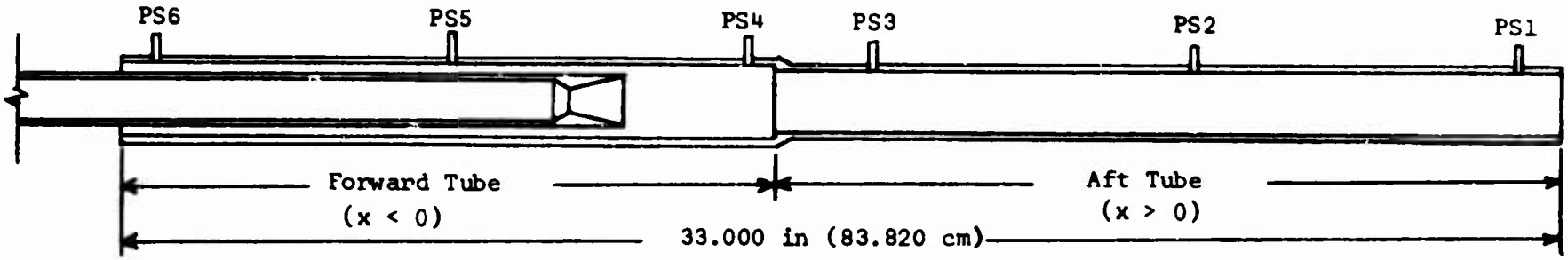

Launcher	Large-diameter forward tube (in./cm.)	Small-diameter aft tube (in./cm.)	r_{aft}/r_{for}	Constrictive area ratio A_{aft}/A_{for}
2	15.000/38.100	18.000/45.720	1.43/1.75	0.668
3	15.016/38.141	17.984/45.679	1.50/1.75	0.735
4	14.965/38.011	18.035/45.809	1.64/1.75	0.878

Pressure tap locations

Tap	$\frac{x}{r_{ne}}$
PS1	30.0
PS2	17.0
PS3	4.0
PS4	-1.0
PS5	-13.0
PS6	-25.0

Figure 4. - The geometries of the constrictive launchers used in the present test program.

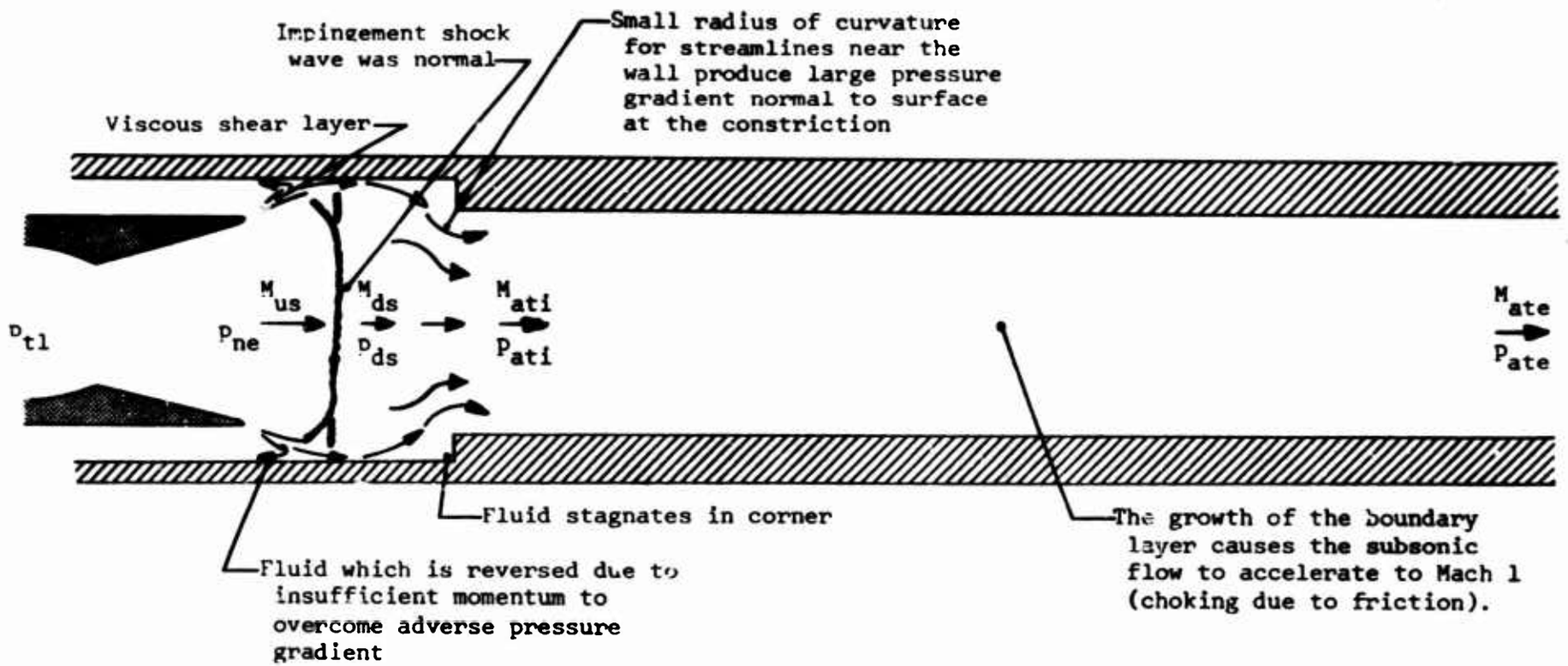

Figure 5. - A sketch of the proposed flow model for conditions where a normal shock wave was generated when the exhaust flow impinged on the wall (i.e., Region 3).

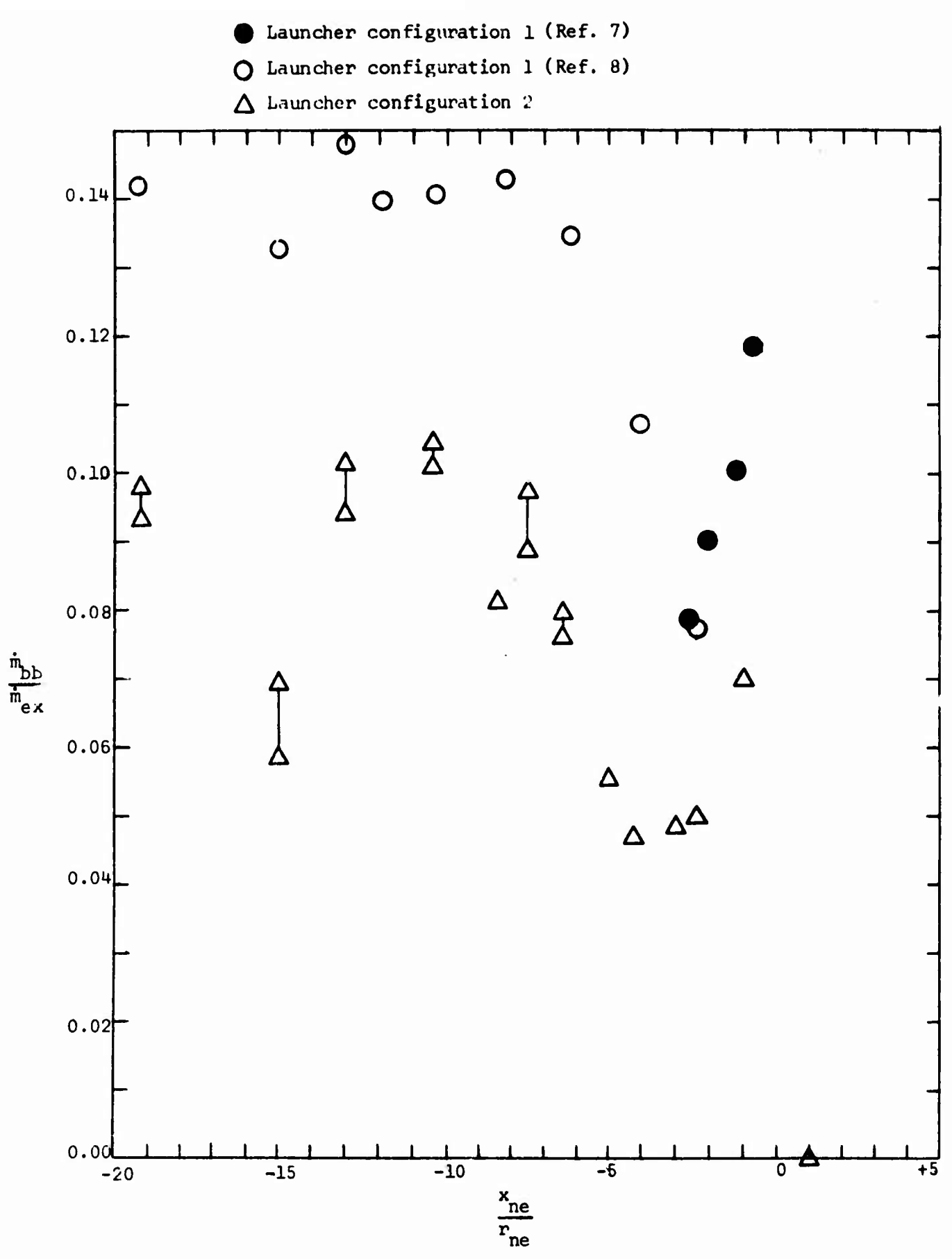

Figure 6. - The nondimensionalized blow-by mass-flow-rate as a function of nozzle exit location for launcher configurations 1 and 2, $p_{t1} \approx 950$ psia (6.55×10^6 N/m^2).

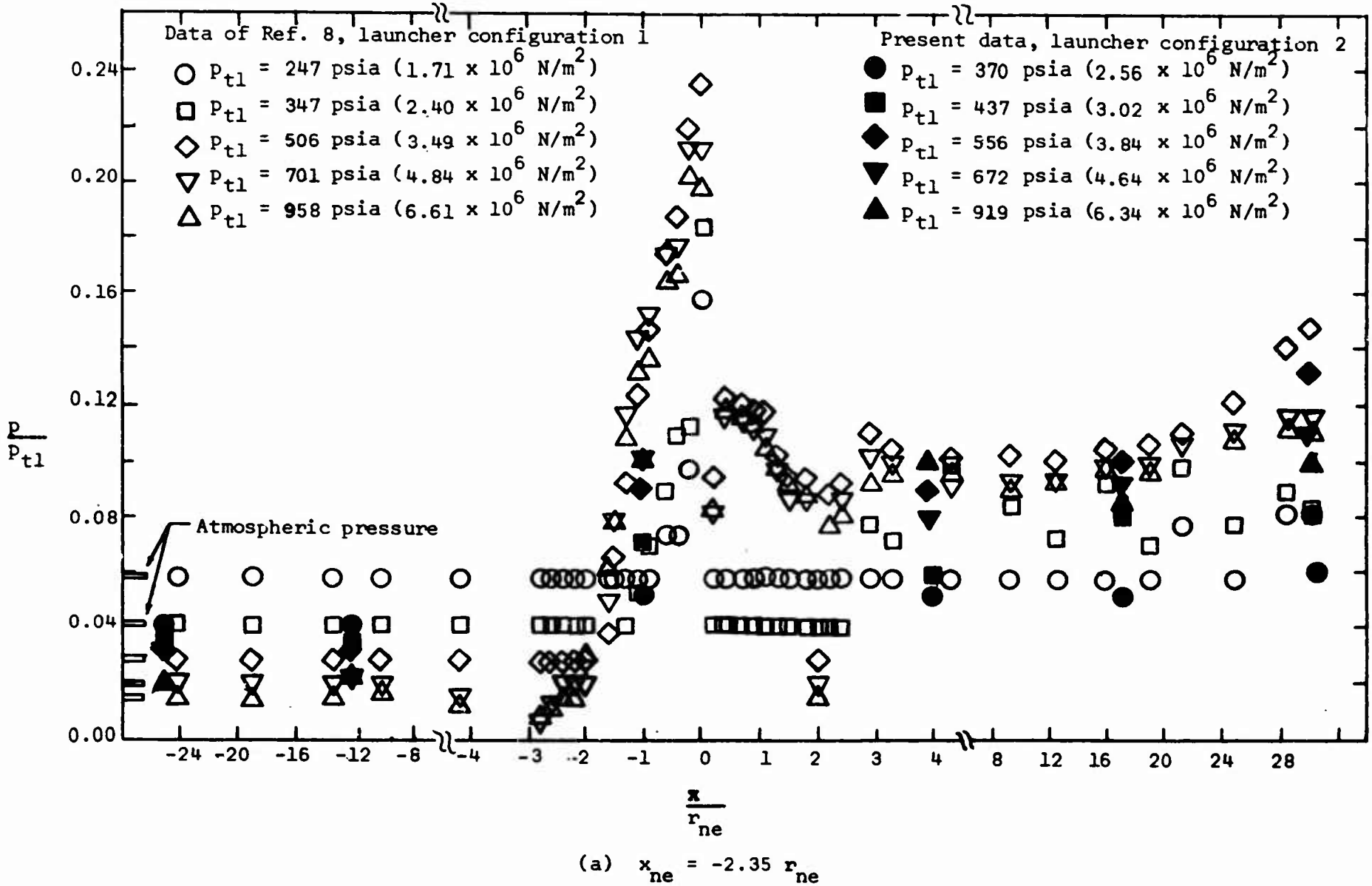

(a) $x_{ne} = -2.35\ r_{ne}$

Figure 7. - The effect of reservoir pressure and nozzle-exit location on the static-wall-pressure distribution obtained for launcher configuration 2.

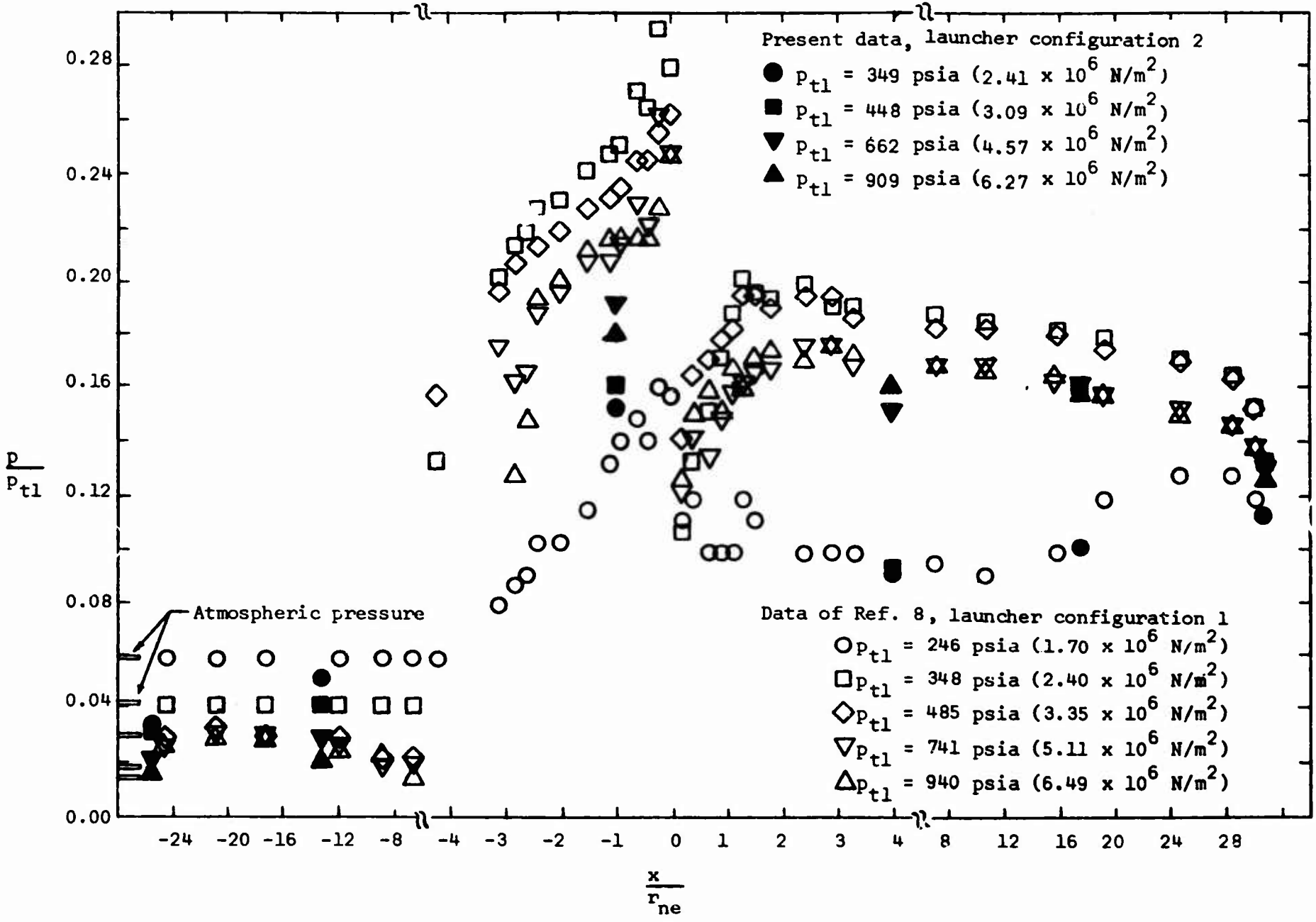

(b) $x_{ne} = -6.41\ r_{ne}$

Figure 7. - Continued.

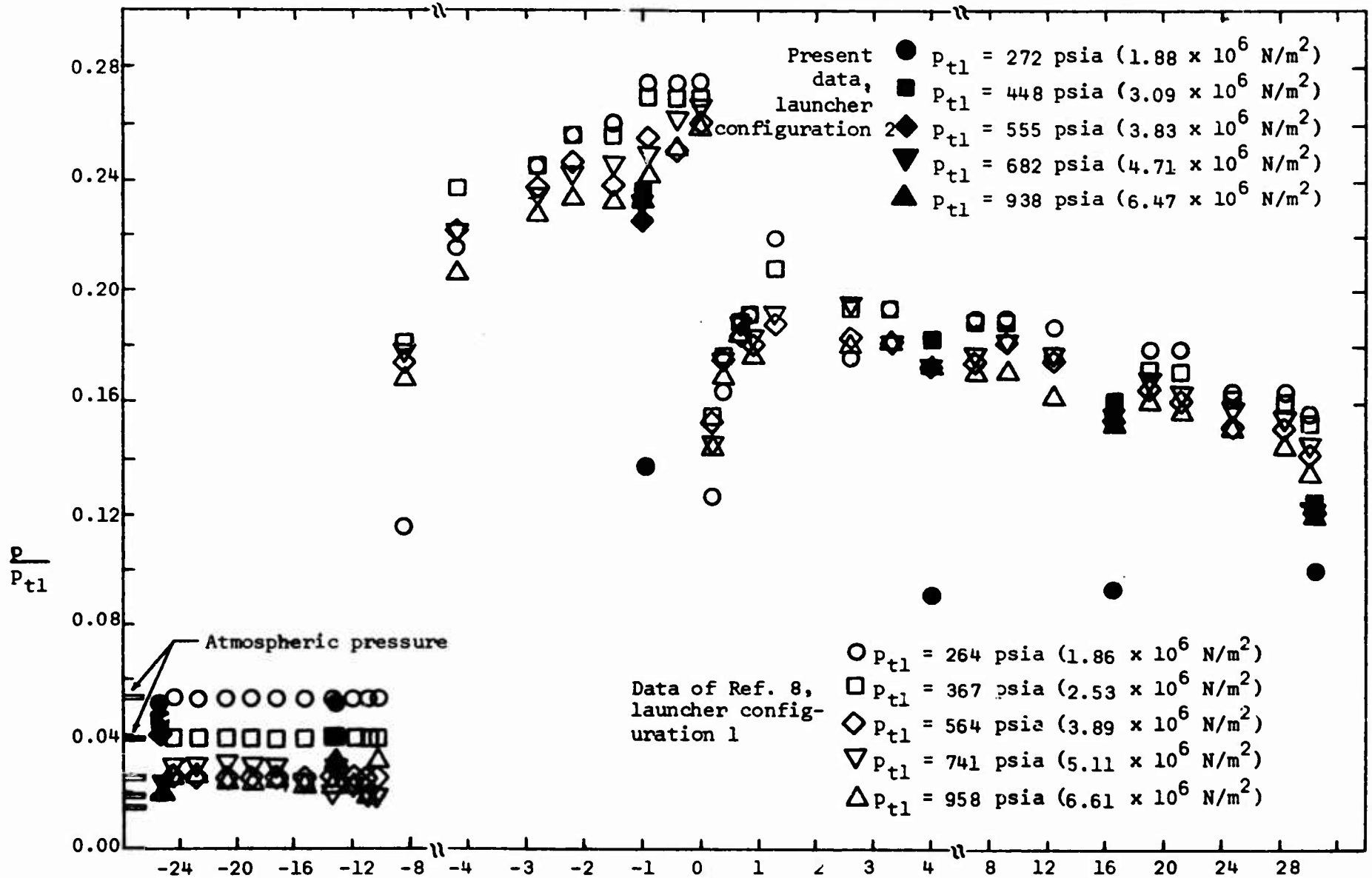

(c) $x_{ne} = -10.41\ r_{ne}$

Figure 7. - Continued.

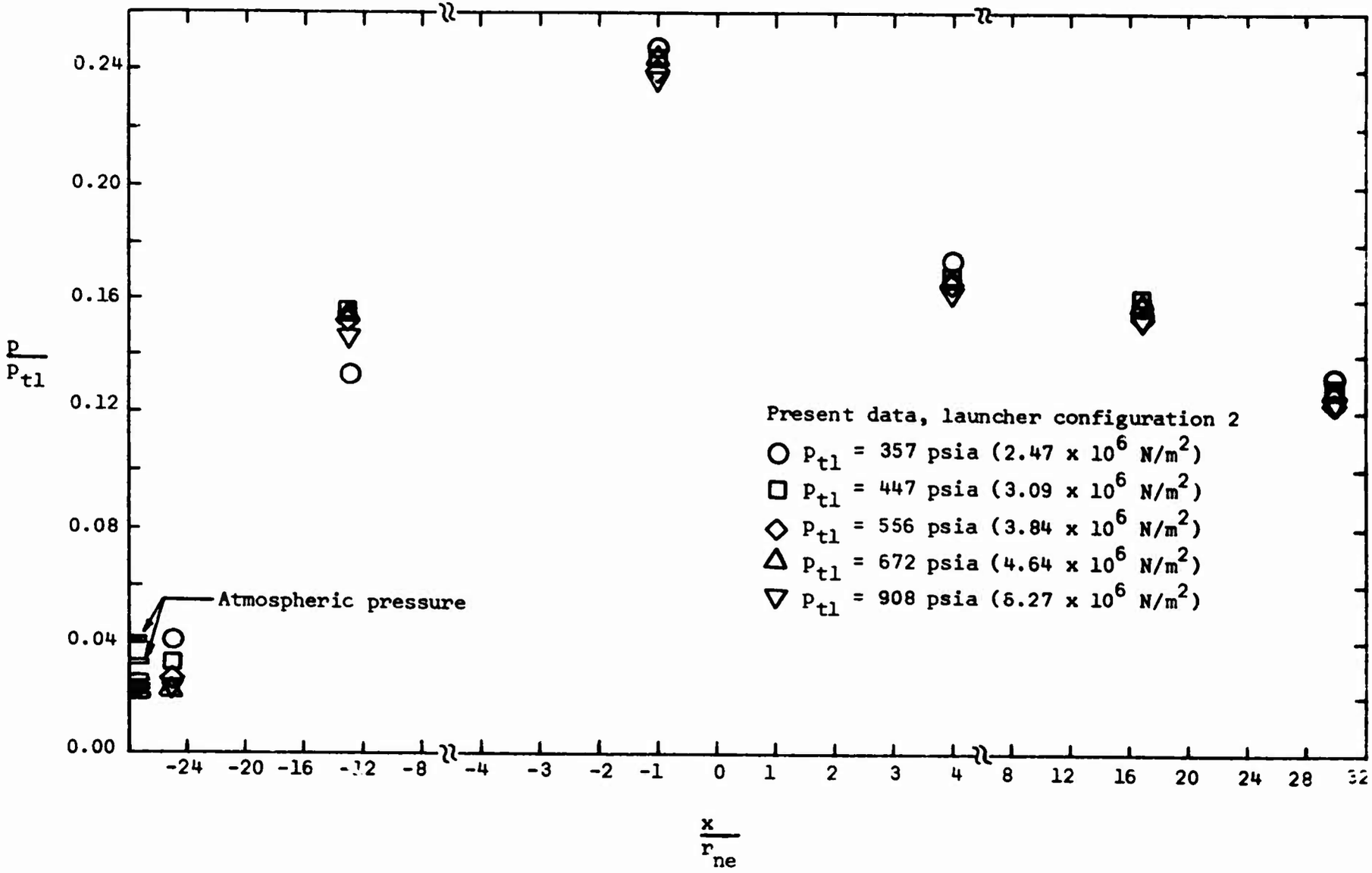

(d) $x_{ne} = -15.00\ r_{ne}$

Figure 7. - Continued.

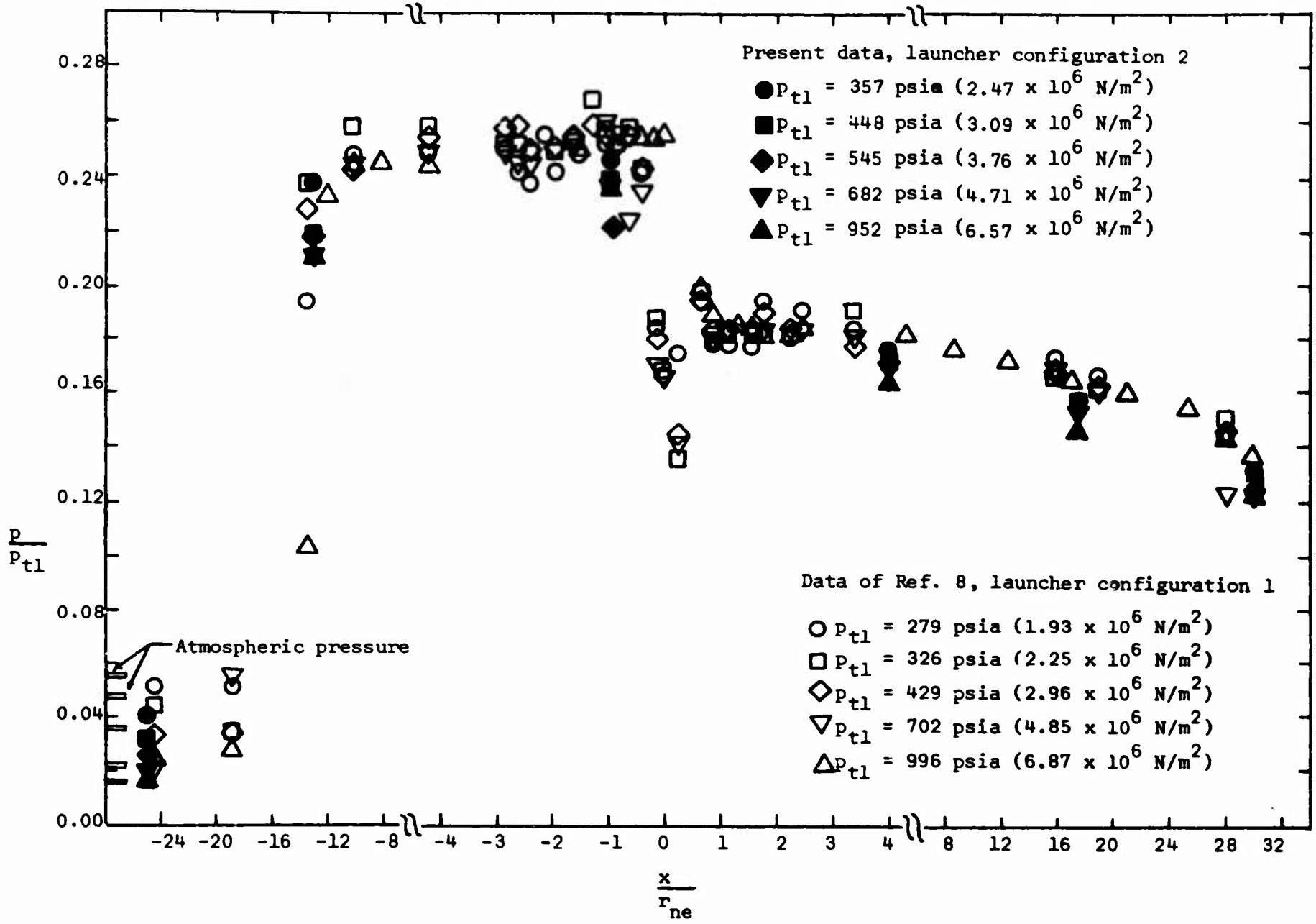

(e) x_{ne} = -19.25 r_{ne}

Figure 7. - Concluded.

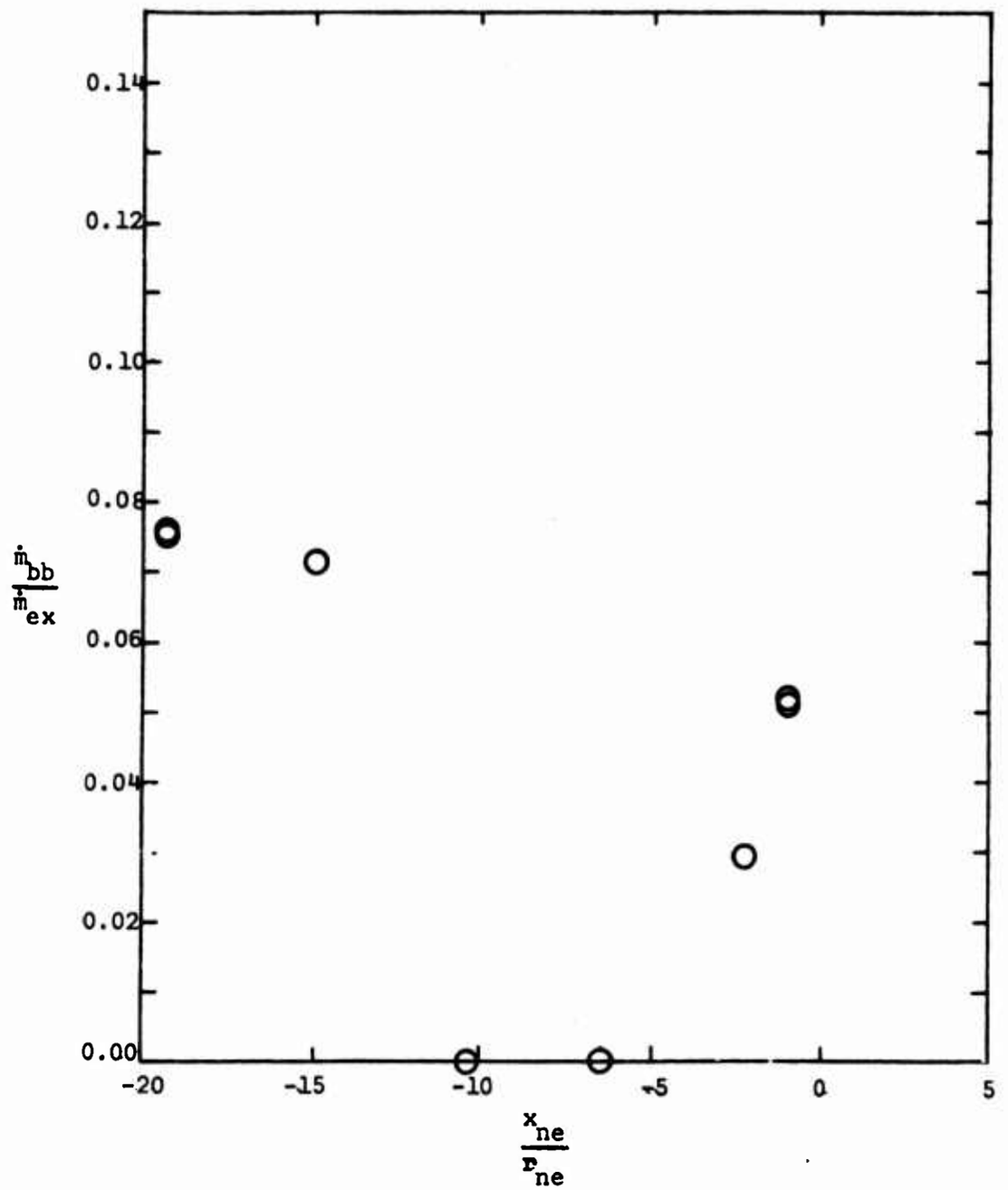

Figure 8. - The nondimensionalized blow-by mass-flow-rate as a function of nozzle exit location for launcher configuration 3, $p_{t1} \sim 950$ psia (6.55×10^6 N/m^2).

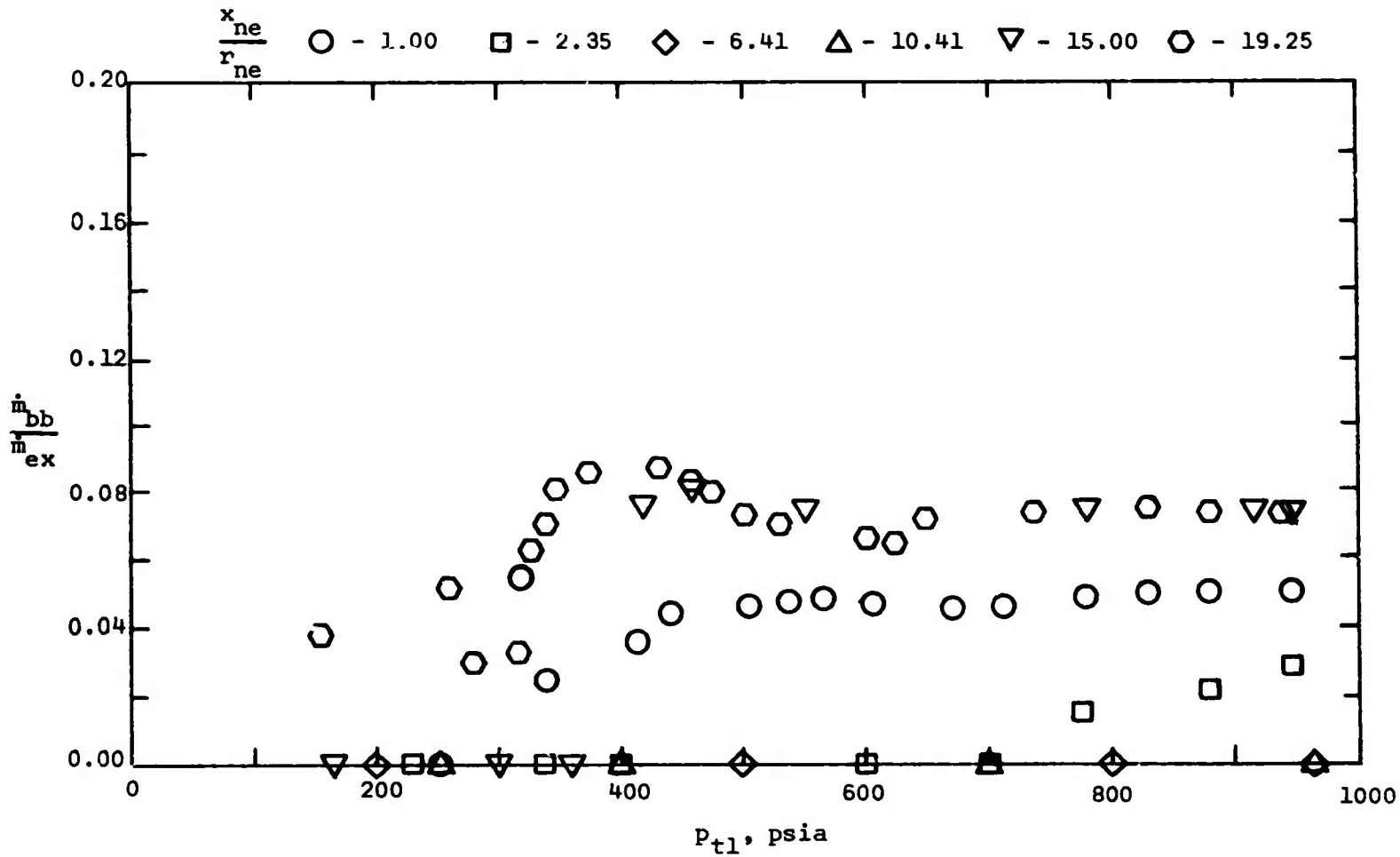

Figure 9. - The nondimensionalized blow-by mass-flow-rate as a function of the reservoir stagnation pressure for launcher configuration 3.

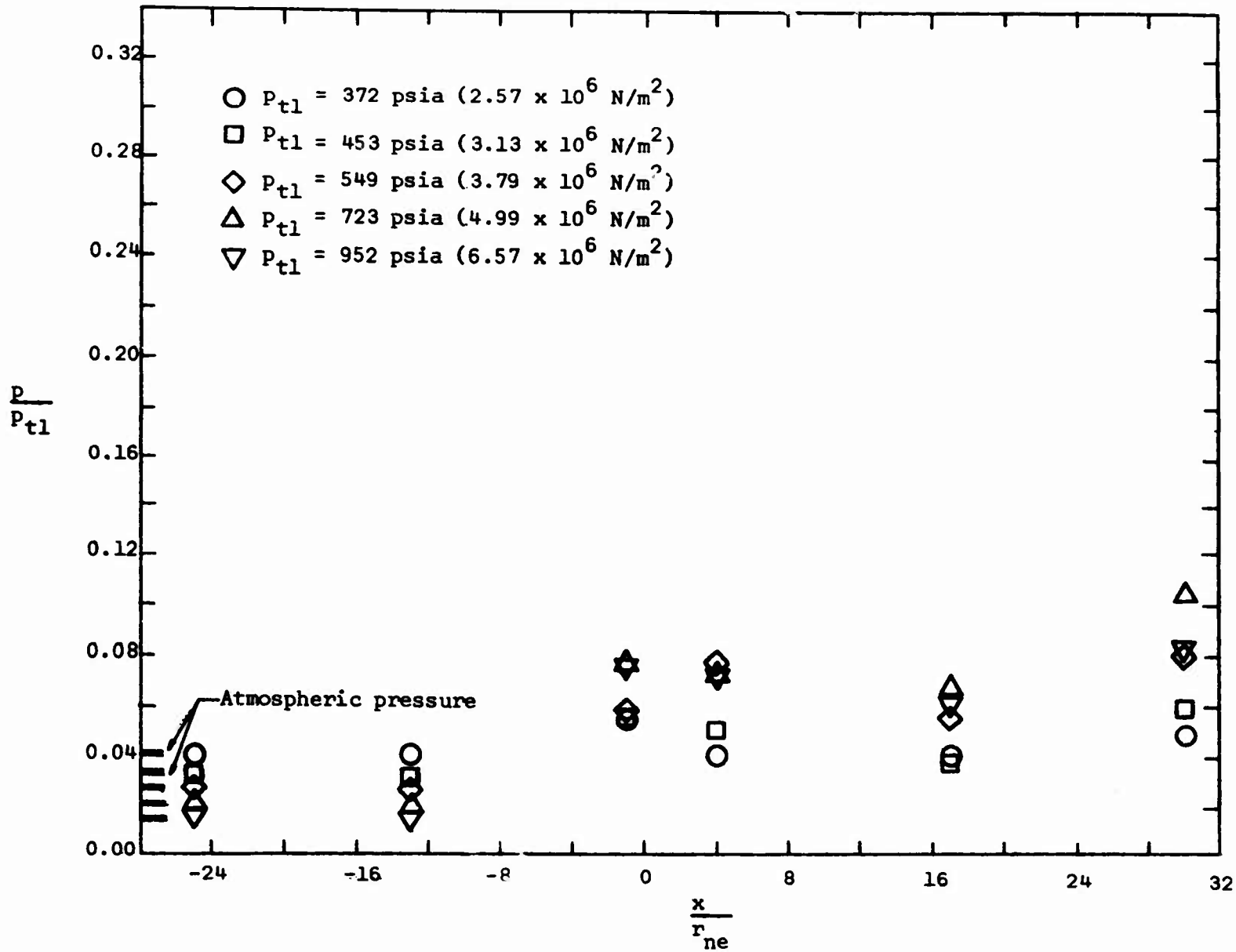

(a) x_{ne} = - 2.35 r_{ne}

Figure 10. - The effect of reservoir pressure and nozzle-exit location on the static-wall-pressure distribution obtained for launcher configuration 3.

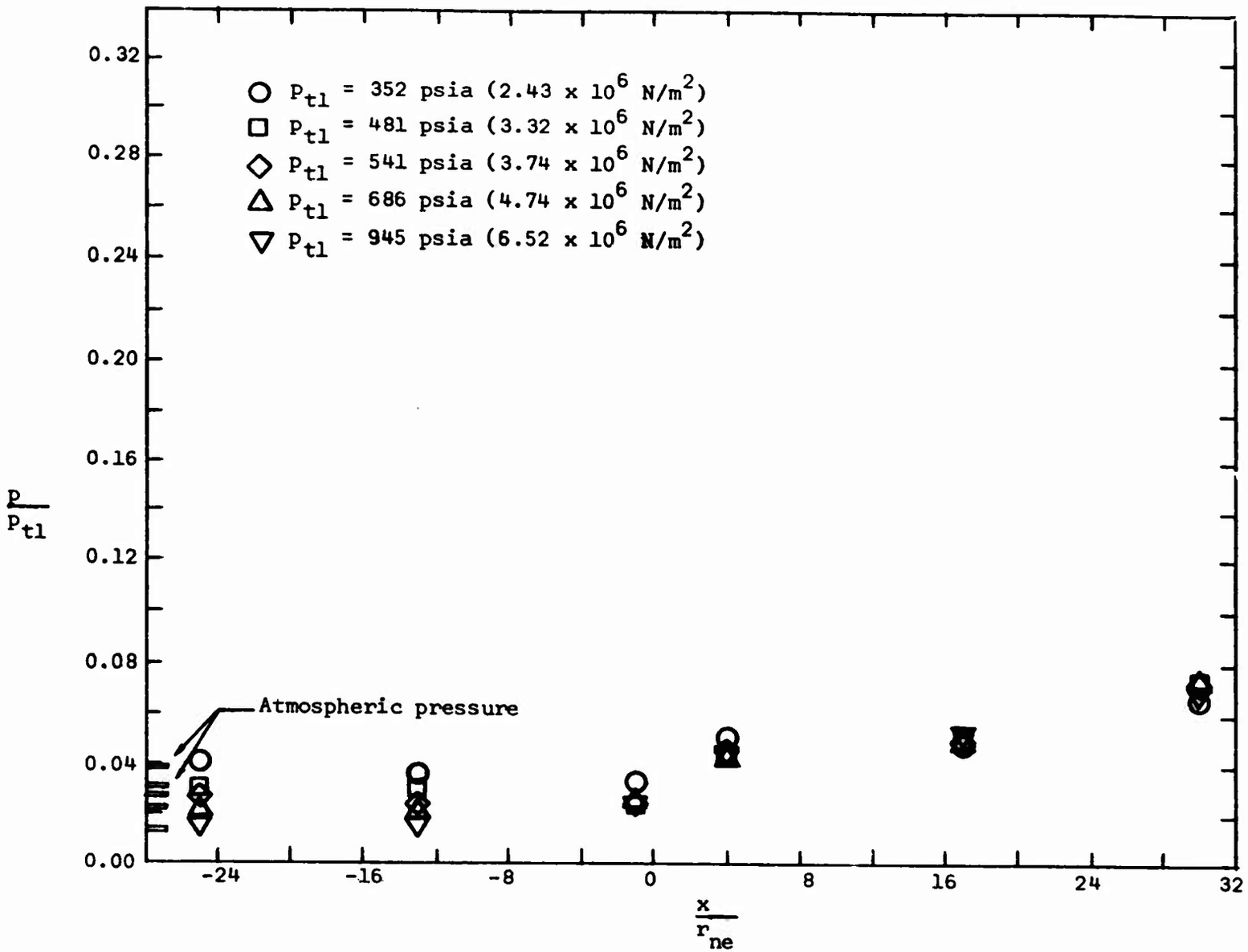

(b) x_{ne} = - 6.41 r_{ne}

Figure 10. - Continued.

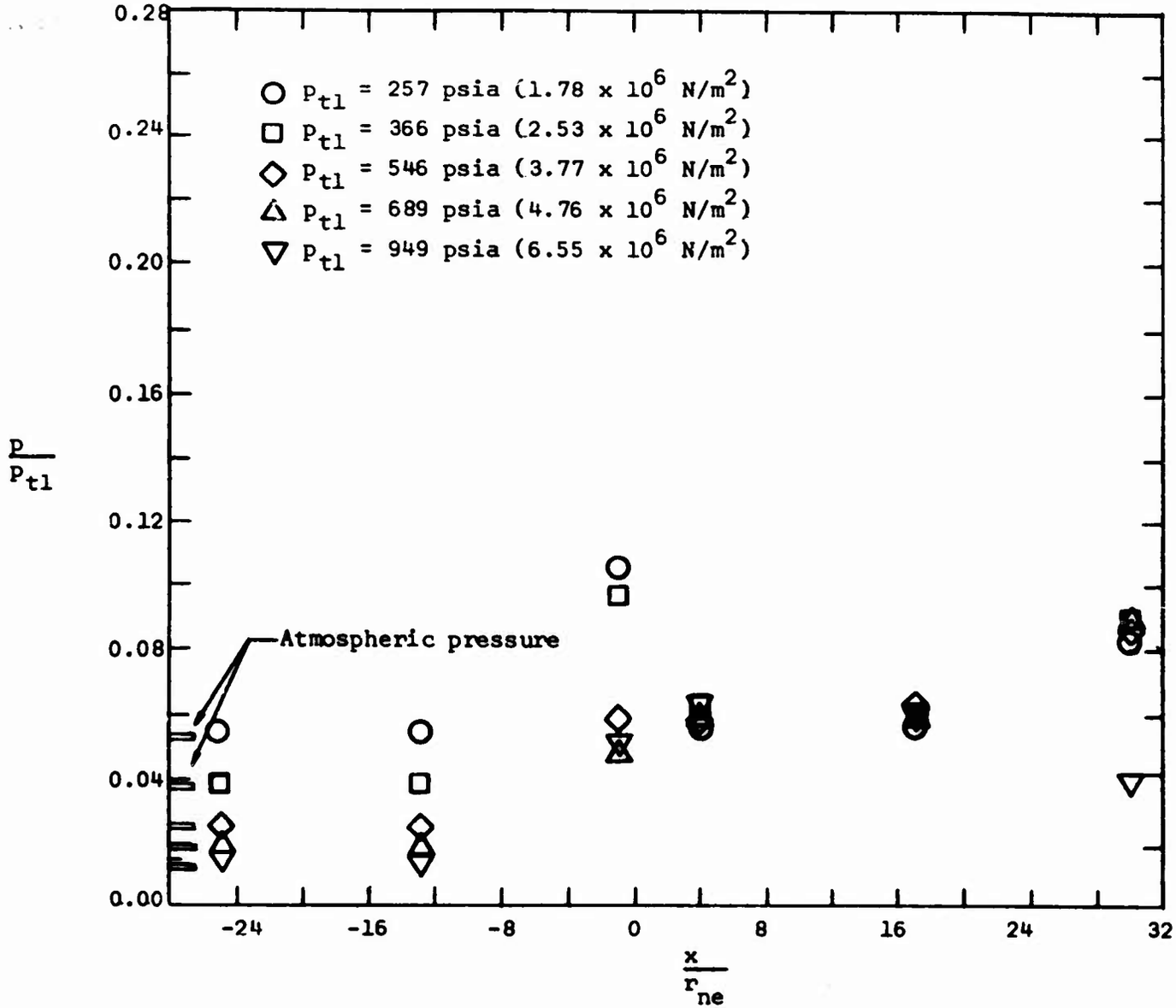

(c) x_{ne} = - 10.41 r_{ne}

Figure 10. - Continued.

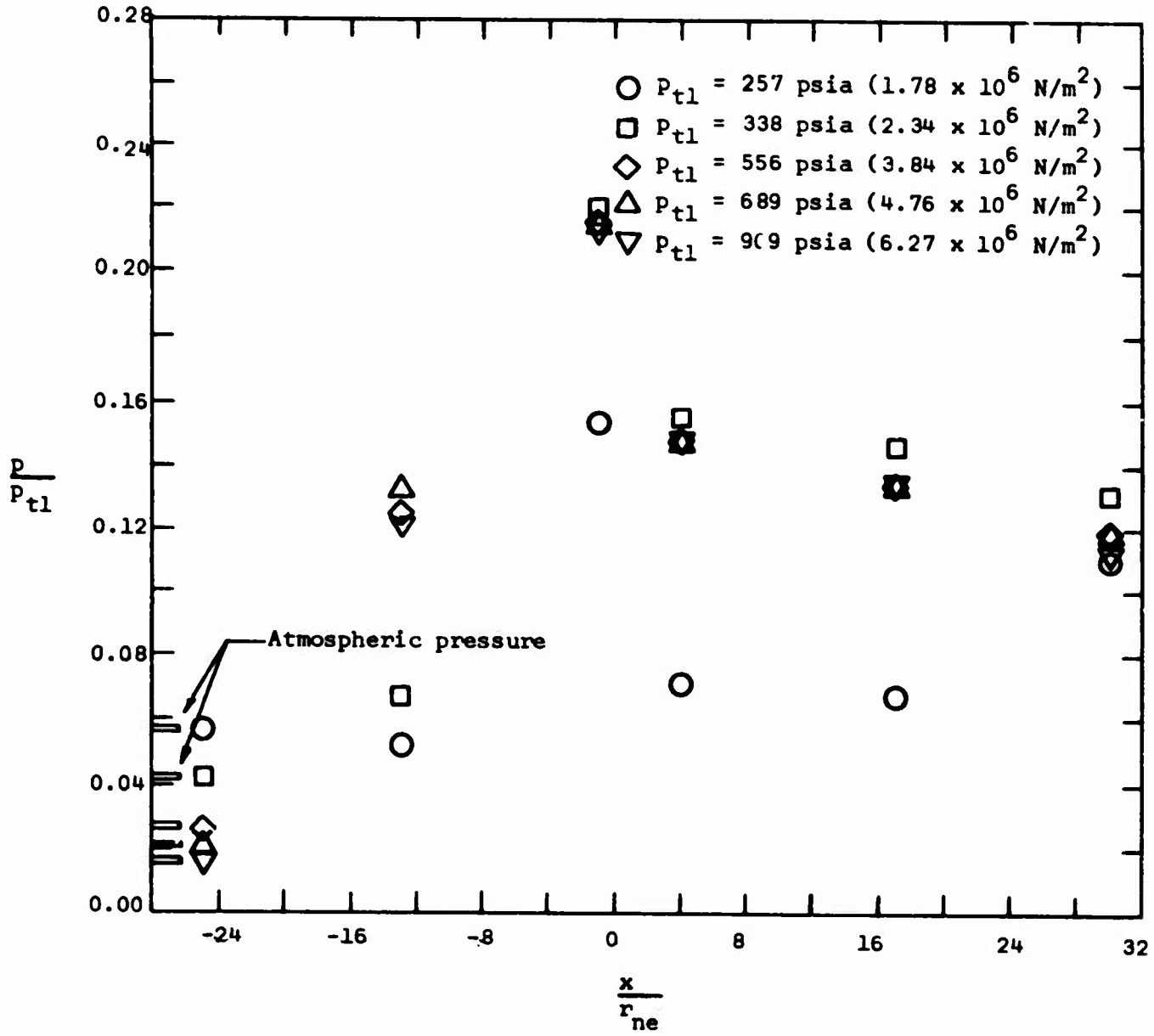

(d) x_{ne} = - 15.00 r_{ne}

Figure 10. - Continued.

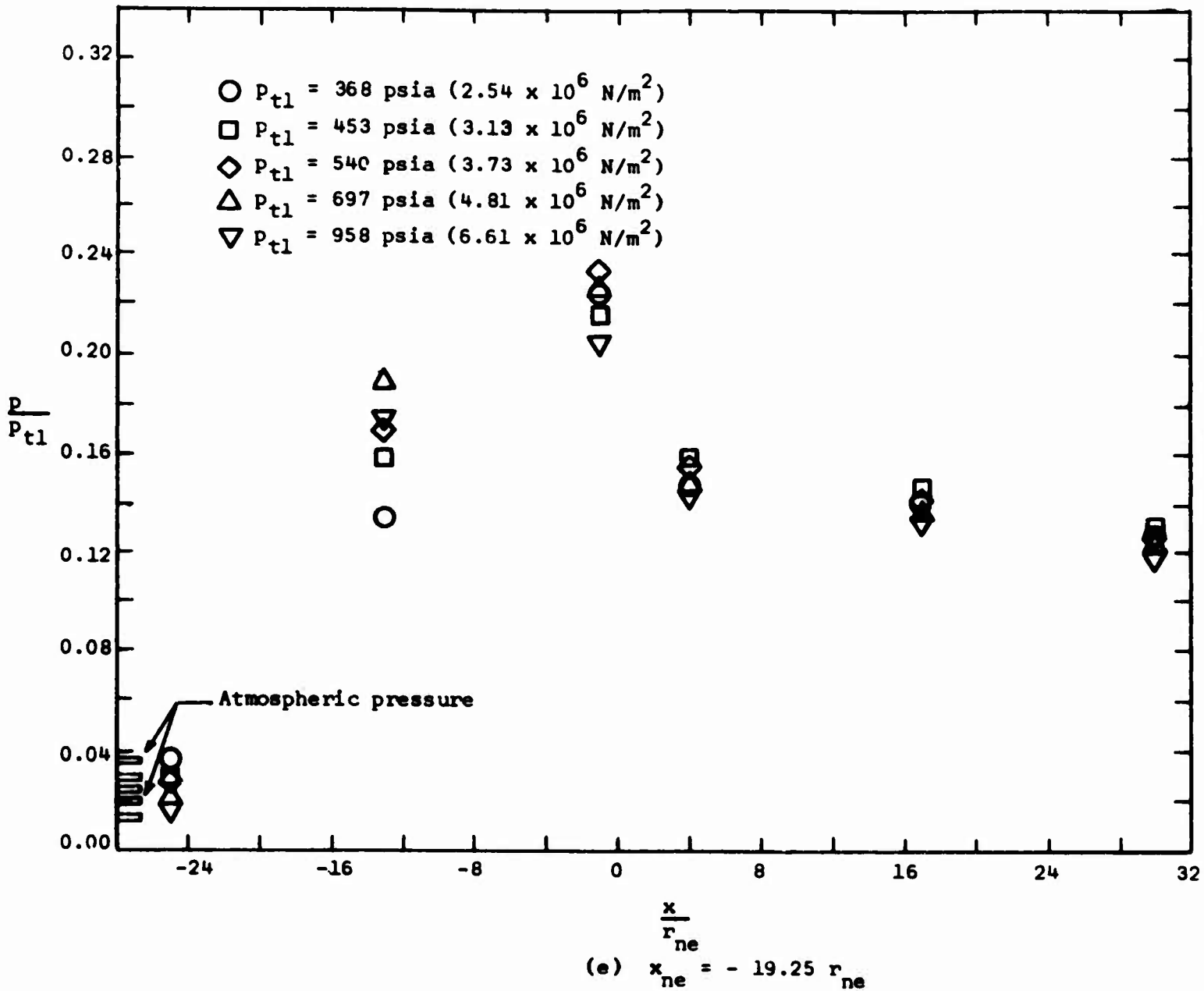

(e) x_{ne} = - 19.25 r_{ne}

Figure 10. - Concluded.

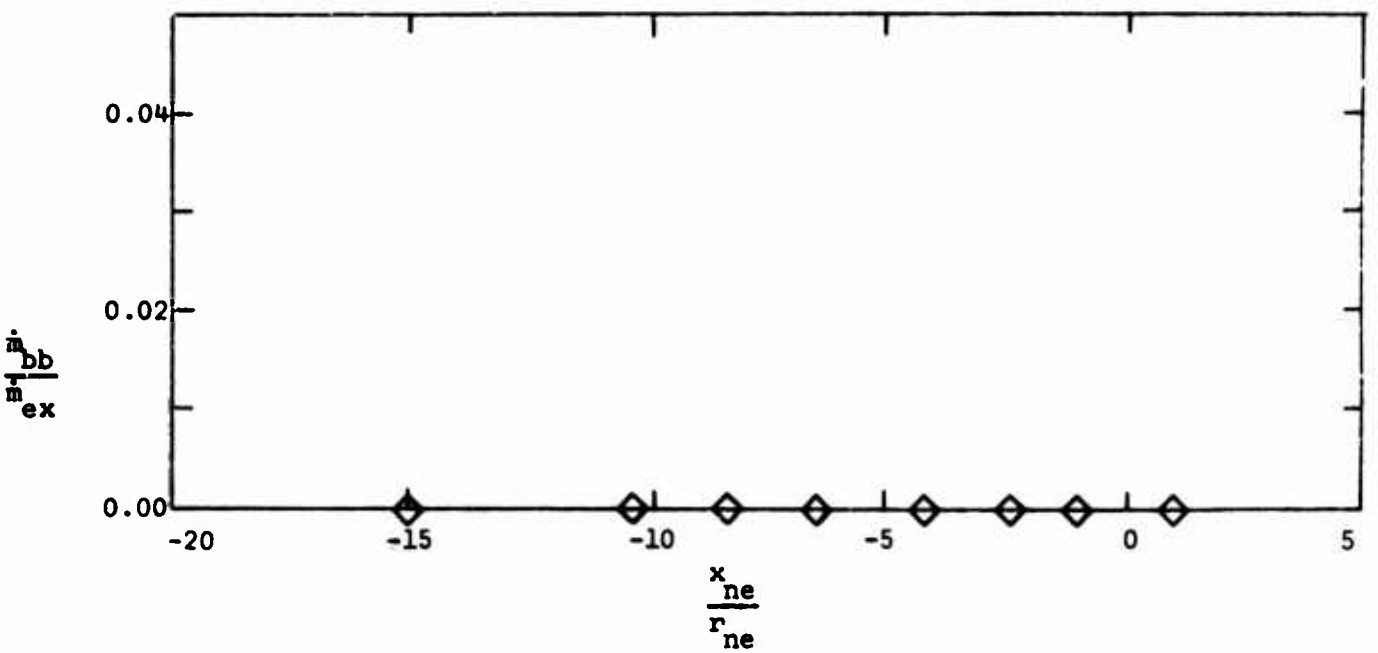

Figure 11. - The nondimensionalized blow-by mass-flow-rate as a function of nozzle-exit location for launcher configuration 4, $p_{t1} \simeq 950$ psia (6.55×10^6 N/m^2).

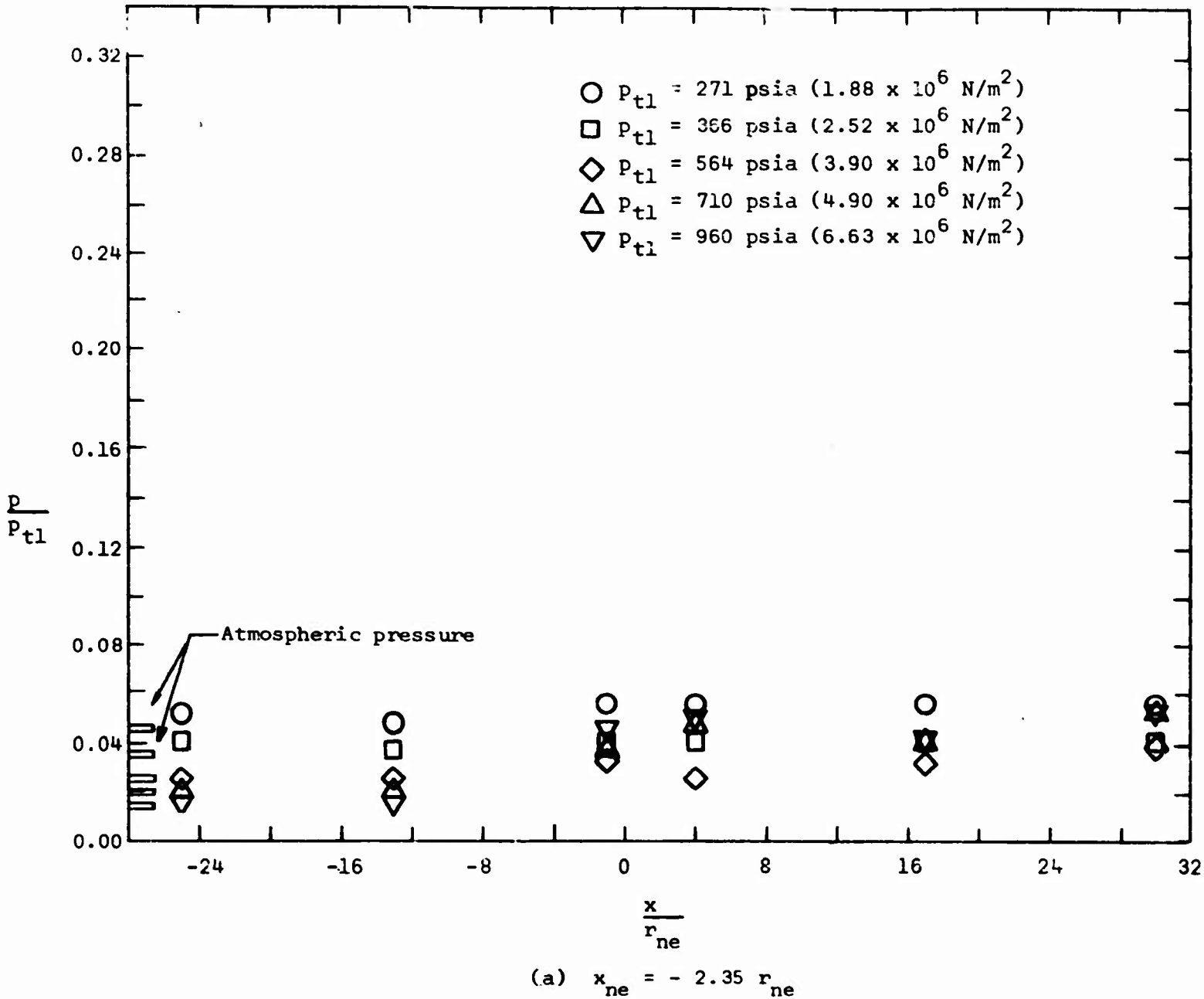

(a) x_{ne} = - 2.35 r_{ne}

Figure 2?. - The effect of reservoir pressure and nozzle-exit location on the static-wall-pressure distribution obtained for launcher configuration 4.

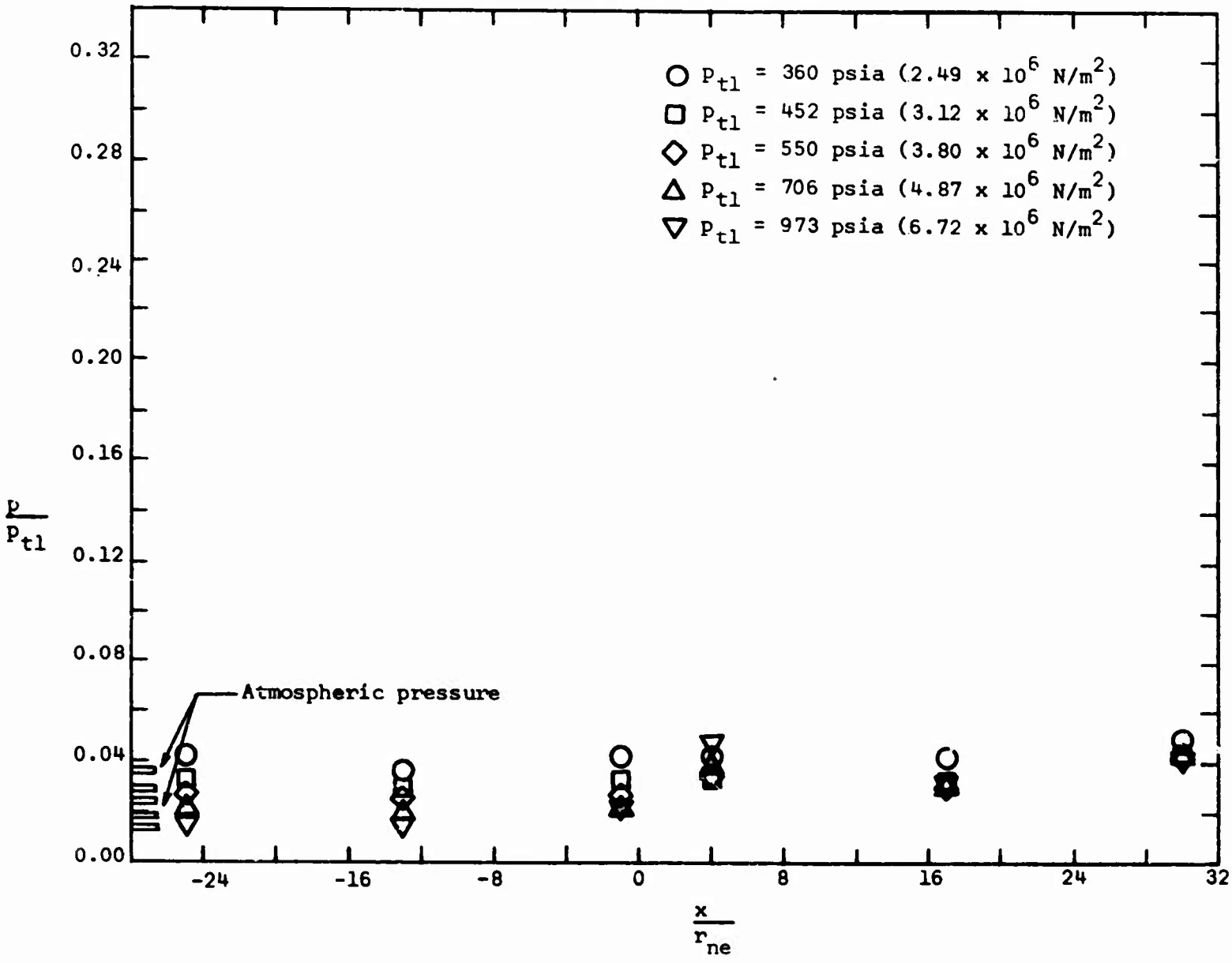

(b) x_{ne} = - 6.41 r_{ne}

Figure 12. - Continued.

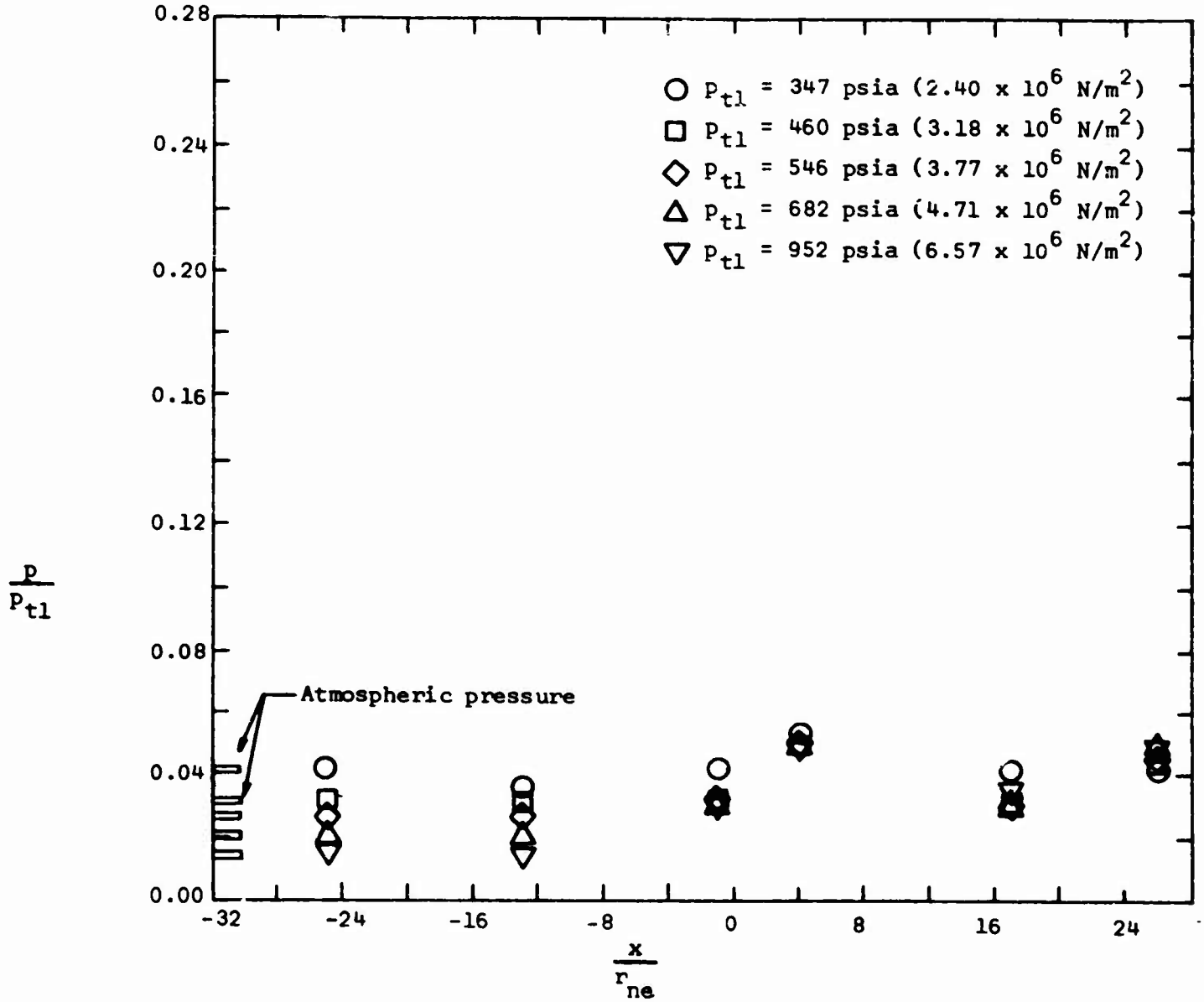

(c) $x_{ne} = -10.41\ r_{ne}$

Figure 12. - Continued.

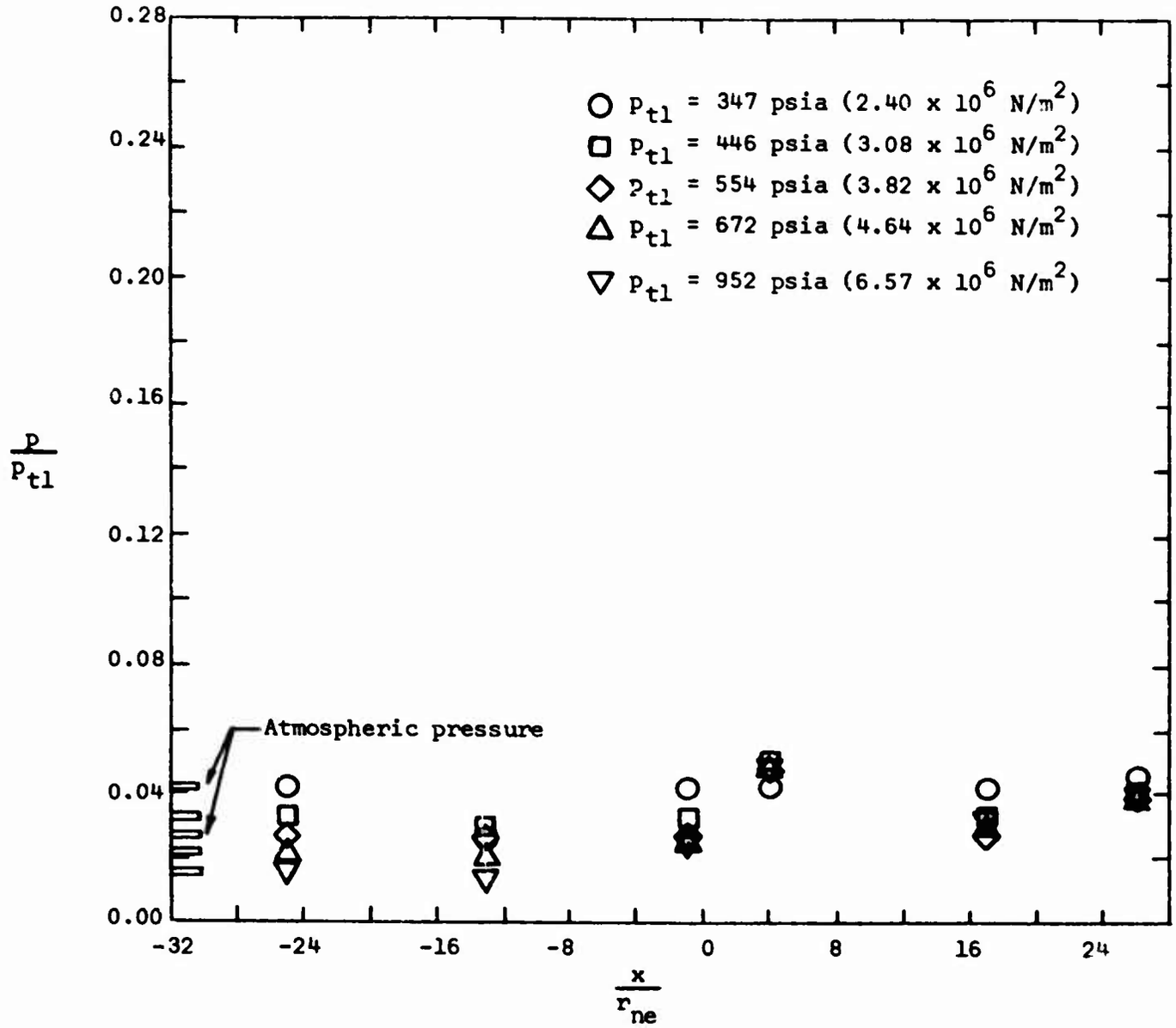

(d) $x_{ne} = -15.00\ r_{ne}$

Figure 12. - Continued.

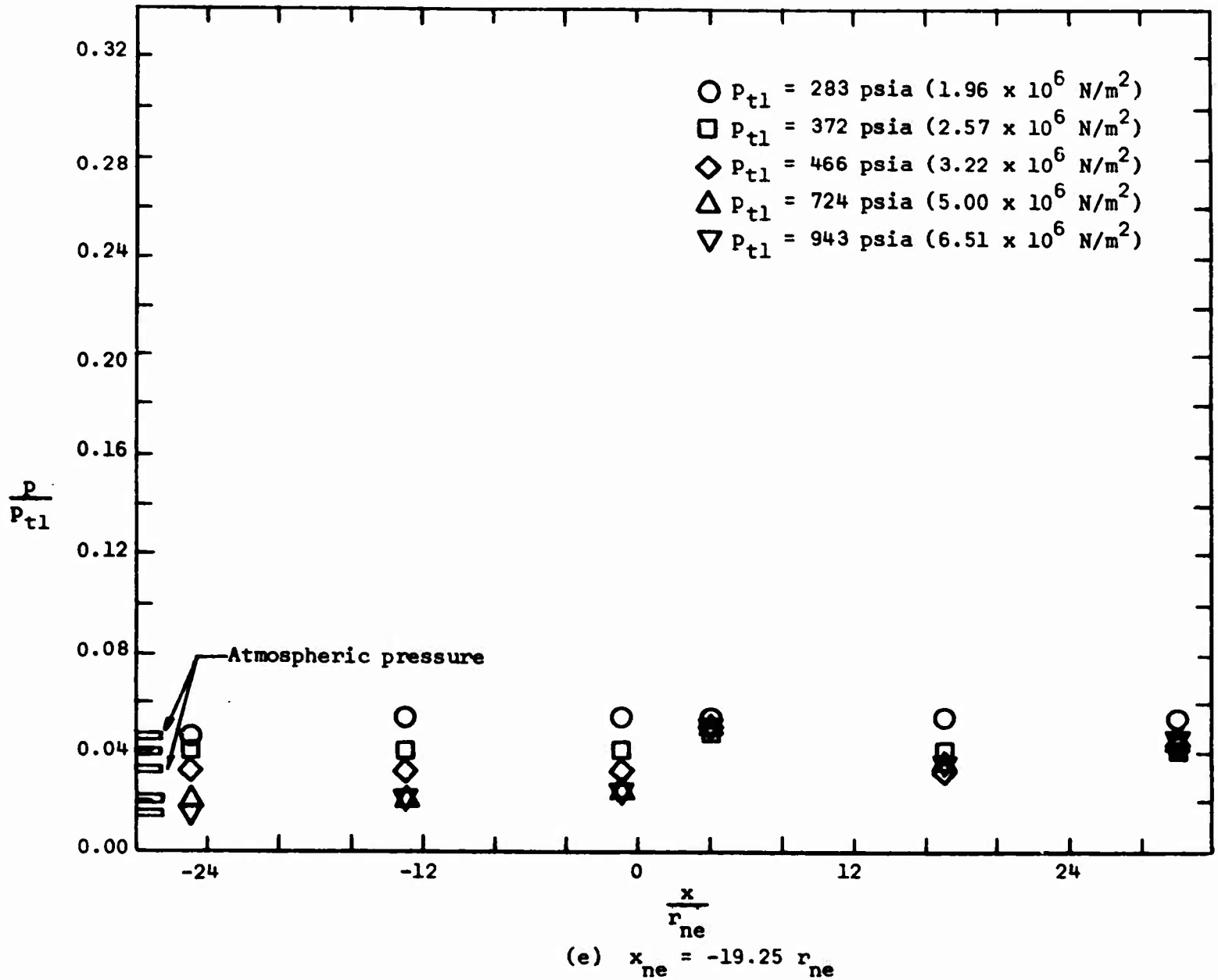

(e) $x_{ne} = -19.25\ r_{ne}$

Figure 12. - Concluded.

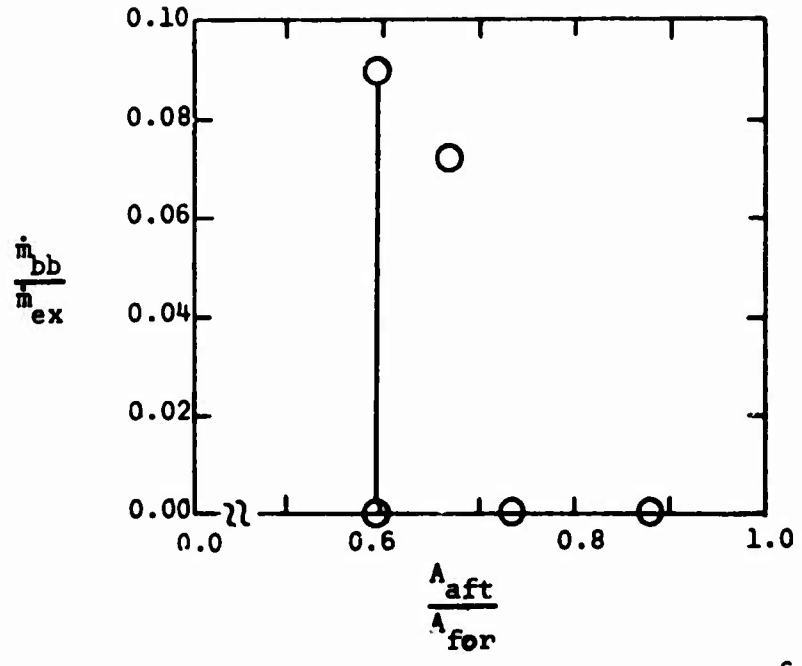

(a) p_{tl} = 400 psia (2.76×10^6 N/m^2)

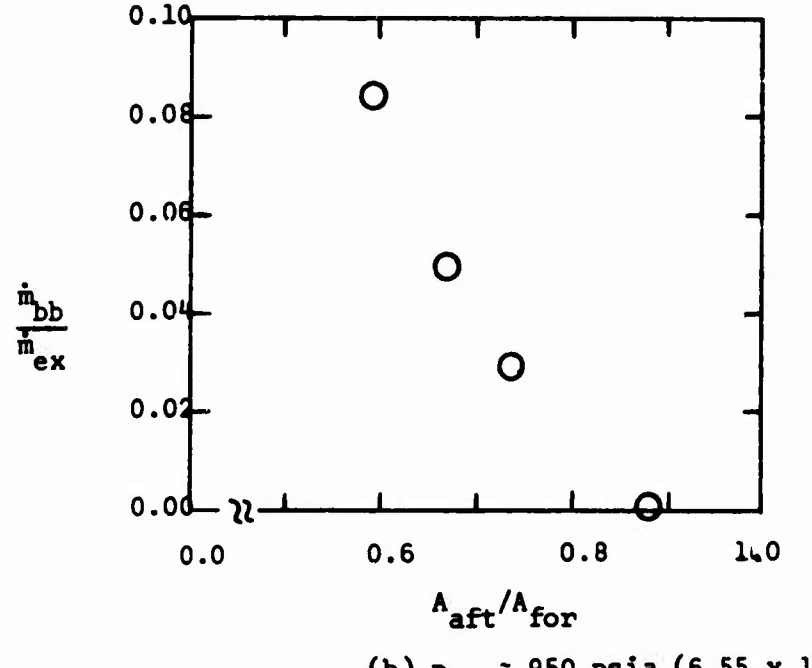

(b) p_{tl} = 950 psia (6.55×10^6 N/m^2)

Figure 13. - The effect of constrictive area ratio on the blow-by mass-flow-rate, $x_{ne} = -2.35\ r_{ne}$.

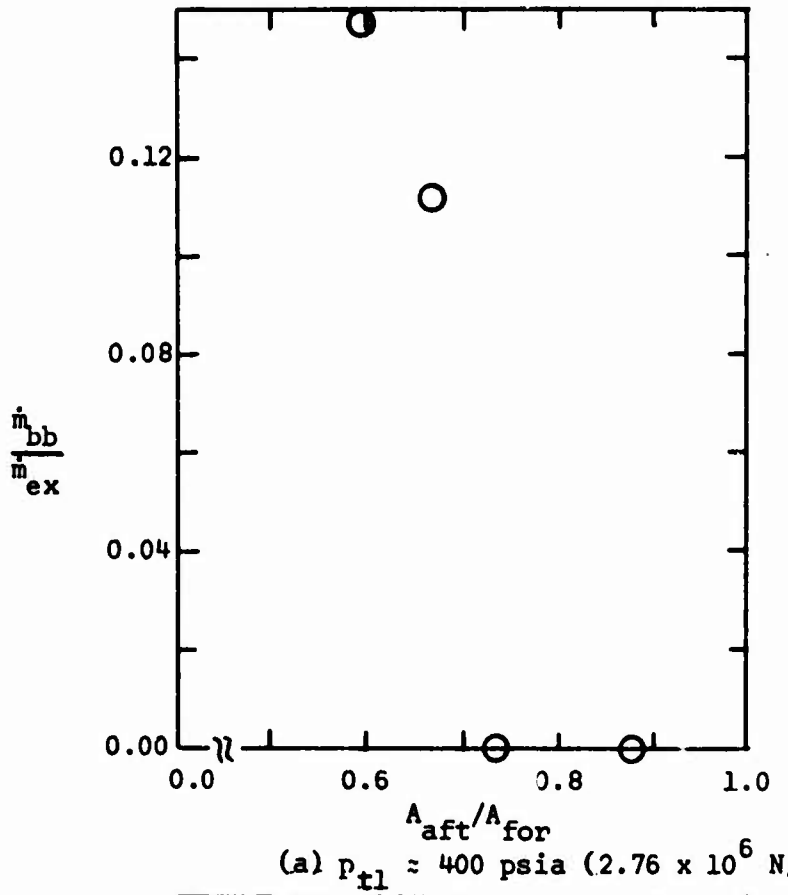

(a) $p_{tl} \approx 400$ psia (2.76×10^6 N/m^2)

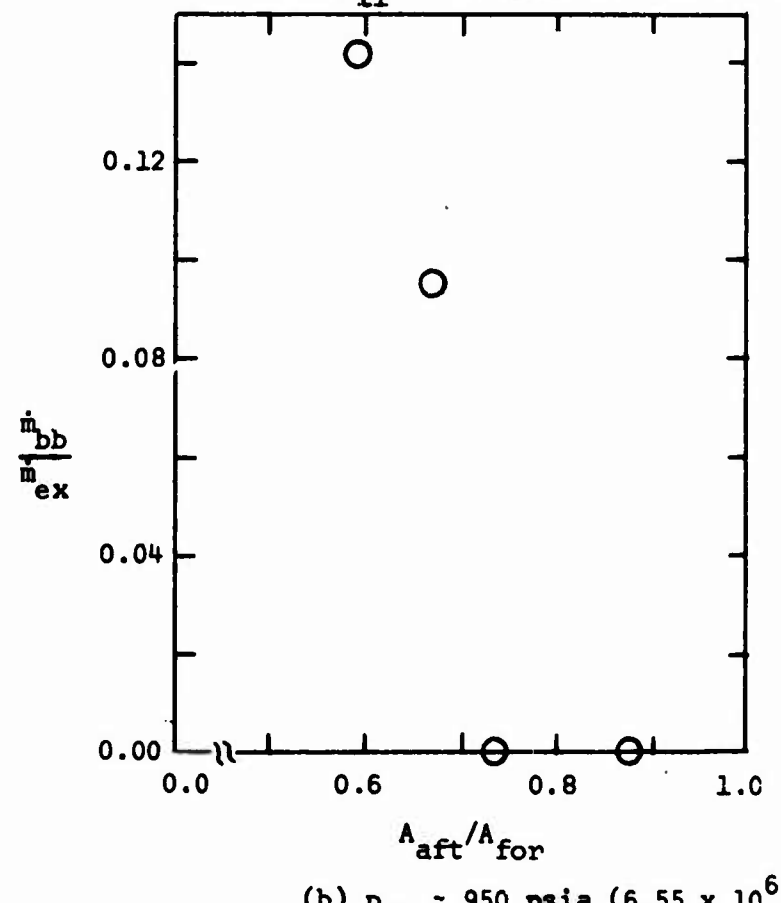

(b) $p_{tl} \approx 950$ psia (6.55×10^6 N/m^2)

Figure 14. - The effect of the constrictive area ratio on the blow-by mass-flow-rate, $x_{ne} = -10.41\ r_{ne}$.

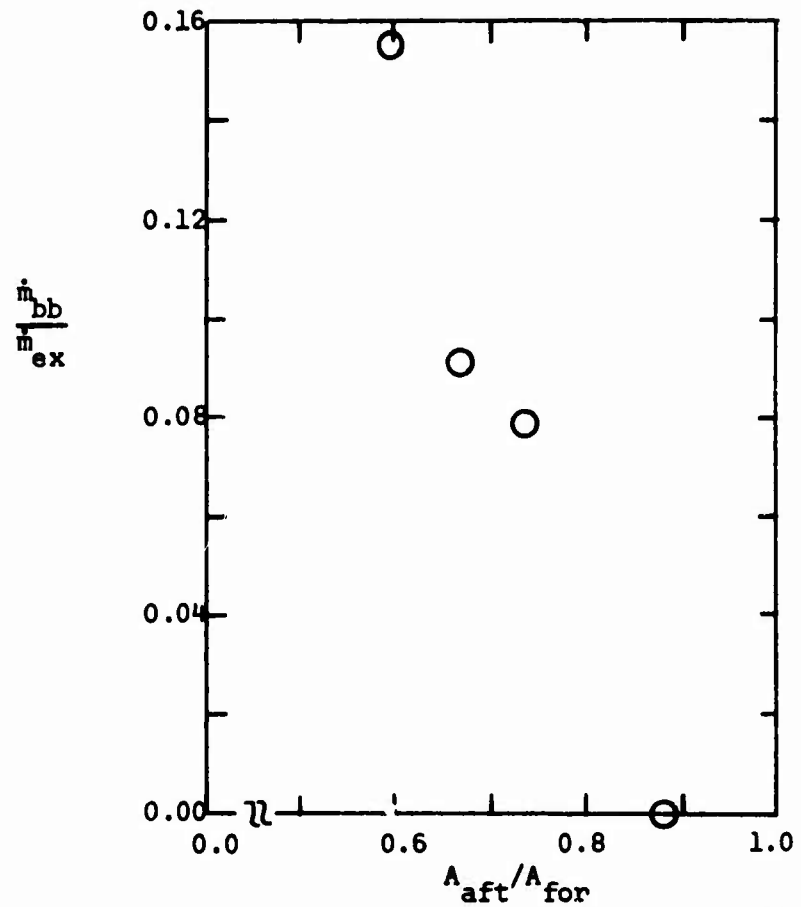

(a) $p_{tl} \simeq 400$ psia (2.76×10^6 N/m^2)

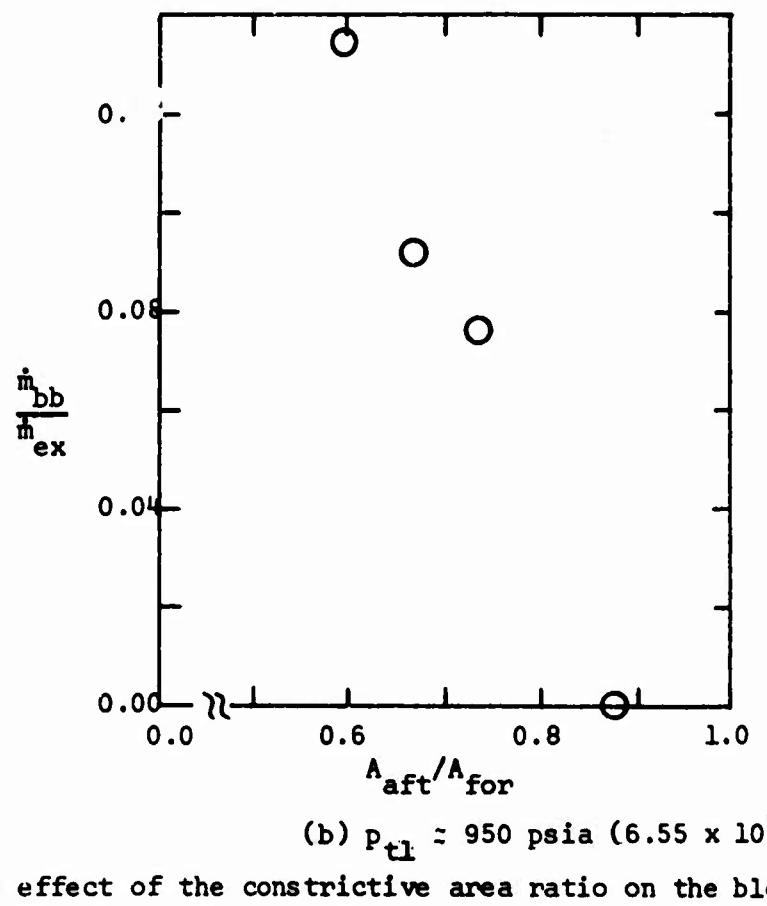

(b) $p_{tl} \simeq 950$ psia (6.55×10^6 N/m^2)

Figure 15. - The effect of the constrictive area ratio on the blow-by mass-flow-rate, $x_{ne} = -19.25\ r_{ne}$.